END
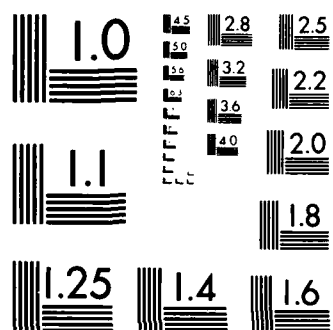
FILMED

DTIC

MICROCOPY RESOLUTION TEST CHART

NATIONAL BUREAU OF STANDARDS 1963 A

FIRST & SECOND QUARTER PROGRESS REPORT 1984

ON PLASMA THEORY AND SIMULATION

January 1 to June 30, 1984

DTIC
ELECTE
JUL 1 7 1985
S   D
A

DTIC FILE COPY

ELECTRONICS RESEARCH LABORATORY

College of Engineering   85 7 15 075
University of California, Berkeley, CA 94720

REPORT DOCUMENTATION PAGE	READ INSTRUCTIONS BEFORE COMPLETING FORM

1. REPORT NUMBER	2. GOVT ACCESSION NO.	3. RECIPIENT'S CATALOG NUMBER
	AD-A156747	

4. TITLE (and Subtitle)	5. TYPE OF REPORT & PERIOD COVERED
Quarterly Progress Report I, II January 1, 1984 - June 30, 1984	Progress, 1/1 - 6/30, 1984
	6. PERFORMING ORG. REPORT NUMBER
	OPR I, II 1984

7. AUTHOR(s)	8. CONTRACT OR GRANT NUMBER(s)
Prof. Charles K. Birdsall	ONR N00014-77-C-0578

9. PERFORMING ORGANIZATION NAME AND ADDRESS	10. PROGRAM ELEMENT, PROJECT, TASK AREA & WORK UNIT NUMBERS
Electronics Research Laboratory University of California Berkeley, CA 94720	Element No. 61153N, Project Task Area RR01-09-01, Work Unit No. NR 012-742

11. CONTROLLING OFFICE NAME AND ADDRESS	12. REPORT DATE
ONR Physics Division Department of the Navy, ONR Arlington, VA 22217	
	13. NUMBER OF PAGES

14. MONITORING AGENCY NAME & ADDRESS(If different from Controlling Office)	15. SECURITY CLASS. (of this report)
	Unclassified
	15a. DECLASSIFICATION/DOWNGRADING SCHEDULE

16. DISTRIBUTION STATEMENT (of this Report)

Approved for public release; distribution unlimited

17. DISTRIBUTION STATEMENT (of the abstract entered in Block 20, If different from Report)

18. SUPPLEMENTARY NOTES

Our group uses theory and simulation as tools in order to increase the understanding of instabilities, heating, transport, and other phenomena in plasmas. We also work on the improvement of simulation both theoretically and practically.

19. KEY WORDS (Continue on reverse side if necessary and identify by block number)

Research in plasma theory and simulation

20. ABSTRACT (Continue on reverse side if necessary and identify by block number)

Theory and Simulation

A. Electron Bernstein wave investigations. Simulations of driving a plasma with these waves, just off perpendicular, (mostly $k_\perp$), has begun, obtaining the predicted damping rate. The objectives are understanding, with potential application to current drive or heating.

B. Simulation of plasma-sheath region, including ion reflection. Using ion reflection at a wall of 70% causes a larger drop in wall sheath potential

(continues other side)

DD FORM 1473 EDITION OF 1 NOV 65 IS OBSOLETE
S/N 0102-LF-014-6601

unclassified

20. ABSTRACT (continued)

    and an increase in the field at the wall. Reflection here means re-emission, i.e., a return as half-Maxwellian.

C. Single ended plasma device, general behavior dc or ac.--This Lausanne ICPP paper describes simulations with various dc biases, showing both stable states (floating, negative bias) and unstable (moderate positive bias) with periodic current disruptions (relaxation oscillations) for both electron and ion rich sources.

D. Single ended plasma device, unstable states.--This Innsbruck Double Layer Conference paper is more detail of the instabilities in C, showing J(t) and phase space for the ion-rich instability.

E. Corrections to time-independent Q-machine equilibria.--In the ion-rich source, negatively biased collector simulations, the classical analysis has an electron hole at the source. However, this hole is filled in the simulations, even when the number of particles is made very large (reducing fluctuations). The corresponding filled-hole analysis fits the measured potentials.

F. Multifluid derivation of the Alfven ion-cyclotron linear dispersion relation. This is an alternative derivation which allows direction connection between features of the wave responsible for the currents and terms in the dispersion relation.

G. Potential barrier between hot and cool plasmas. These simulations are aimed at explaining the experimental observation of a potential dip between hot and cool plasmas. So far no spatial interface has been observed.

Code Development

A. PDW1, Particle simulation of non-periodic (bounded) systems. The code is out, with a User's Manual, in heavy use here (see A,B,C,D,E,G above) and available to others.

TABLE OF CONTENTS

Page No.

FIRST AND SECOND QUARTER PROGRESS REPORT
ON
PLASMA THEORY AND SIMULATION

January 1 to June 30, 1984

Our research group uses both theory and simulation as tools in order to increase the understanding of instabilities, heating, transport, and other phenomena in plasmas. We also work on the improvement of simulation, both theoretically and practically.

Our Staff is -

Professor C. K. Birdsall   191M   Cory Hall   (642-4015)
Principal Investigator

Dr. Thomas L. Crystal   187M   Cory Hall   (642-3477)
Post-Doctorate; Lecturer, UCB

Dr. Bruce Cohen   L630   LLNL   (422-9823)
Dr. A. Bruce Langdon   L477   LLNL   (422-5444)
Dr. William Nevins   L630   LLNL   (422-7032)
Adjunct Lecturers, UCB; Physicists LLNL

Dr. Mary Hudson   SSL   (642-1327)
Guest, UCB; Senior Fellow,
         Space Science Lab.

Mr. Perry Gray   119ME   Cory Hall   (642-3528)
Senior Engineering Aide

Mr. Kwang-Youl Kim
Mr. William Lawson
Mr. Niels Otani
Ms. Lou Ann Schwager
Mr. Vincent Thomas
Research Assistants   119MD   Cory Hall   (642-1297)
                              119ME   Cory Hall   (642-3528)

June 30, 1984

A.   # ELECTRON BERNSTEIN WAVE INVESTIGATIONS

Wm. S. Lawson and *J. P. Lynov (visitor, Riso, Denmark)*

A modification of the code PDW1 is being used to investigate the properties of oblique Bernstien waves at finitesimal amplitudes. So far, the code has been shown to work, and reproduce Bernstein waves with the correct damping rate (for oblique angles). A significant wave number shift has been noted, however, for relatively small excitations.

The numerical experiment is modeled on the Double Plasma experiment of Armstrong, Rasmussen, Stenzel, and Trulsen [1]. The exciter is composed of three grids, the outer two being tied together, and being voltage driven with respect to the center grid. This experimental model may be responsible for some peculiar effects observed at *low* amplitudes, such as the apparent reflection of the driven wave.

Other effects observed, but not explained are the apparent excitation of waves at *higher* frequencies than the driving frequency, and reduced damping at high amplitude. Work is continuing in an attempt to explain these results.

An ongoing problem is the relatively high noise level of the simulations. This noise seems to be associated with the high dimensionality of the simulation (1-D, 3-V), and has dictated large numbers of particles and time averaging.

[1] Armstrong et. al., *Physics Letters* 85A(1981)281-284.

B.   SIMULATION OF THE PLASMA-SHEATH REGION
                           INCLUDING ION REFLECTION

              Lou Ann Schwager (Prof. C. K. Birdsall, Dr. I. Roth)

A low temperature plasma interacts with a collector plate primarily through charged particle reflection, emission, or absorption. These phenomena will affect the electric potential profile and hence the transport to the plate. Present simulation studies indicate that a reflected ion current increases the plasma potential above that simulated with a purely absorbing plate.

The computer code **PDW1** models this behavior. The setup of this simulation is identical to that described in the previous report (**QPR** III,IV 1983). This earlier study modelled plasma flowing into a purely absorbing plate. The current work differs from the previous only in the inclusion of ion reflection at the plate. The system is shown in Figure 1. As in the earlier run, ions and electrons returning to the source are thermalized and re-injected with the initial flux. We have chosen a mass ratio of 40 to conserve computation time and an ion reflection coefficient of 70%. This coefficient represents those parameters which are typical of the plasma region at the collector plate in the end cell of a tandem mirror reactor (and possibly in the poloidal divertor of a tokamak).

For a hydrogen plasma with temperatures of 30-100 eV incident on a plate of molybdenum, the atomic data in Table 1 pertains.

Table 1. Atomic Data for 30-100 eV H on Mo

Mechanism	Interaction Coefficient
Reflected Ion * per Ion	.6-.8 [1]
Secondary Electron per Electron	.4-.8 [2]
Reflected Electron per Electron	.05-.10 [2]
Secondary Electron per Ion	0 [2]
Sputtered Mo atom per Ion (1 keV)	2×10^{-3} [2]

* It was later discovered that only a small fraction of the reflected particles are ionized. This will be accounted for in later reports.

Obviously the plate does not behave as a purely absorbing boundary. We model ion reflection here because it dominates the other mechanisms. In future work we intend to include others from Table 1.

Unfortunately, little information is available on the reflection of low energy light ions. *Oen* and *Robinson*[1] used the simulation program **MARLOWE** to derive universal curves for the reflection coefficients of various light ions independent of target material. They plot the reflection coefficient as a function of the Thomas-Fermi reduced energy, ϵ. The formula they use is

$$\epsilon = \frac{0.03EM}{zZ(m+M)(z^{2/3}+Z^{2/3})^{1/2}}$$ [3]

where m and M are the projectile and target atomic weights, z and Z are the projectile and target atomic numbers, and E is the projectile energy in eV. Hence, for energies of 30-100 eV, protons hitting a Mo target have ϵ ranging from 0.02 to 0.006. With this range for ϵ, Figure 6 of Reference 2 specifies that the ion reflection coefficient lies between 60% and 80%.

Electric potential histories at $x = L/2$ for reflection coefficients of 0% and 70% are shown in Figures 2A and 2B. Electrons reaching the wall before ions cause the early potential rise in both cases. The interaction of the opposing ion flows prior to equilibration, seen in Figure 3A, generates the perturbed potential profile in Figure 3B. This appears as a mild transient in the potential in Figure 2B. After equilibration, the opposing ion flows lead to the mildly perturbed potentials, as shown in Figure 4A. This results in the nearly flat potential profile of Figure 4B. Note also in Figure 3B that the 70% case generates a steeper potential profile in the sheath region (where $E_{wall} = -19$) than that for the 0% case in Figure 4C (where $E_{wall} = -5.8$). The steep potential rise away from the wall repels low energy reflected ions at $x = 0$. The ion excess in the sheath then generates an even stronger electric field.

Our next steps are to include the study of a reflected flux, which depends on the incident flux and energy, and of the effects of secondary electron emission.

References
1. O.S.Oen and M.T.Robinson, "Computer Studies of the Reflection of Light Ions from Solids", *Nuclear Instruments and Methods* 132, pp.647-653 (1976).
2. C.F.Barnett *et al*, "Atomic Data for Controlled Fusion Research", Oak Ridge National Laboratory, Oak Ridge, Tennessee, ORNL-5207, pp.D.1.8-D.5.13 (1977).
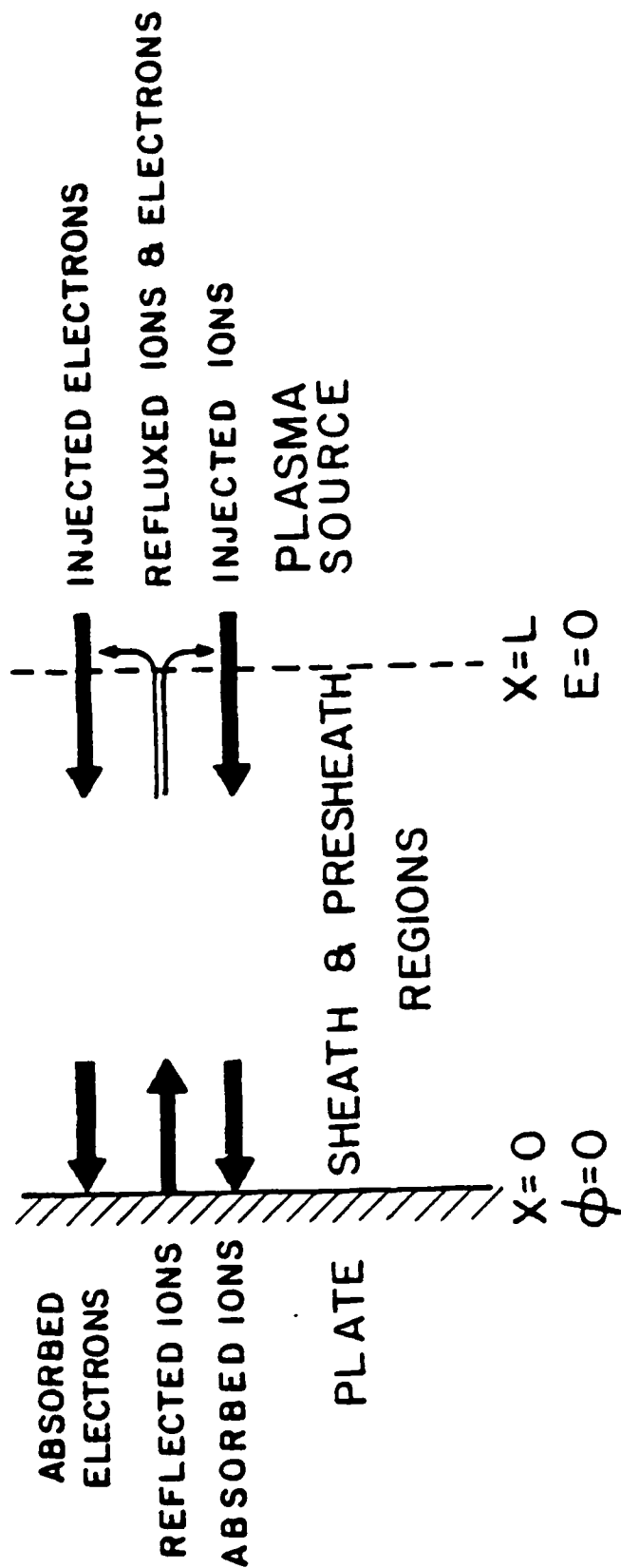3. T.J.Dolan, *Fusion Research*, Vol III, Pergamon Press, New York, 1980, p.697.
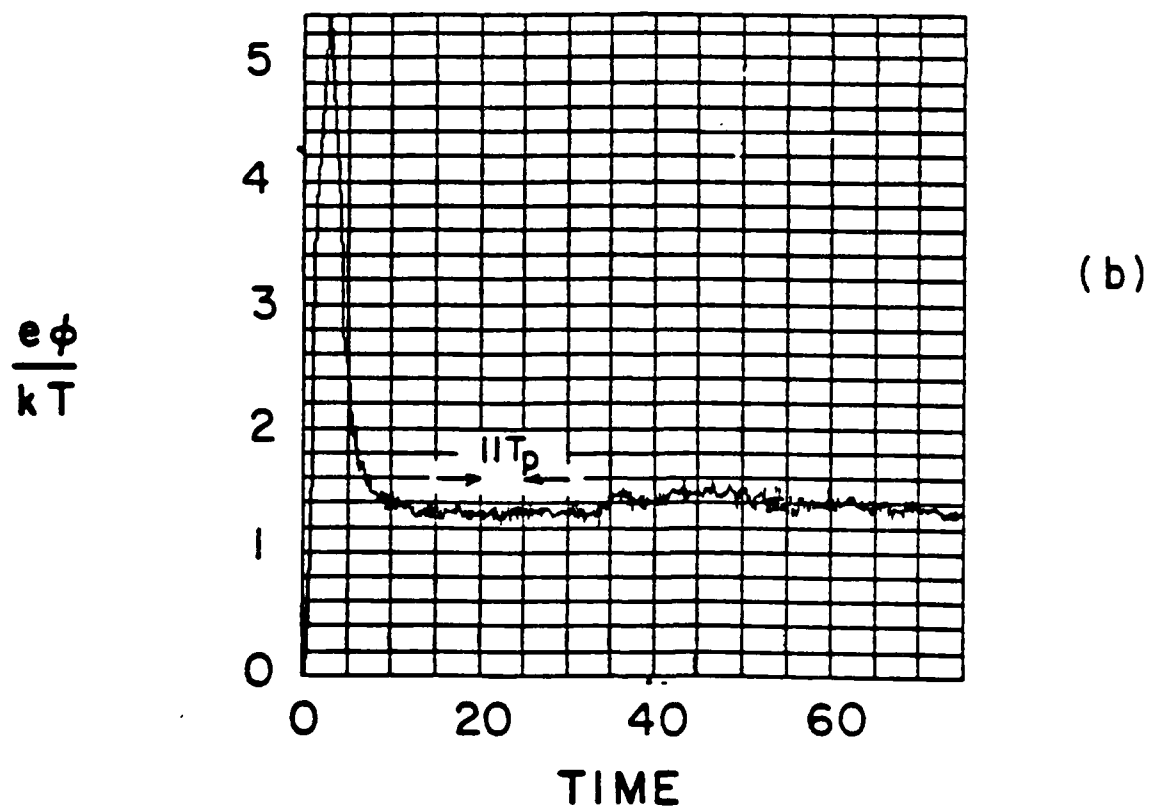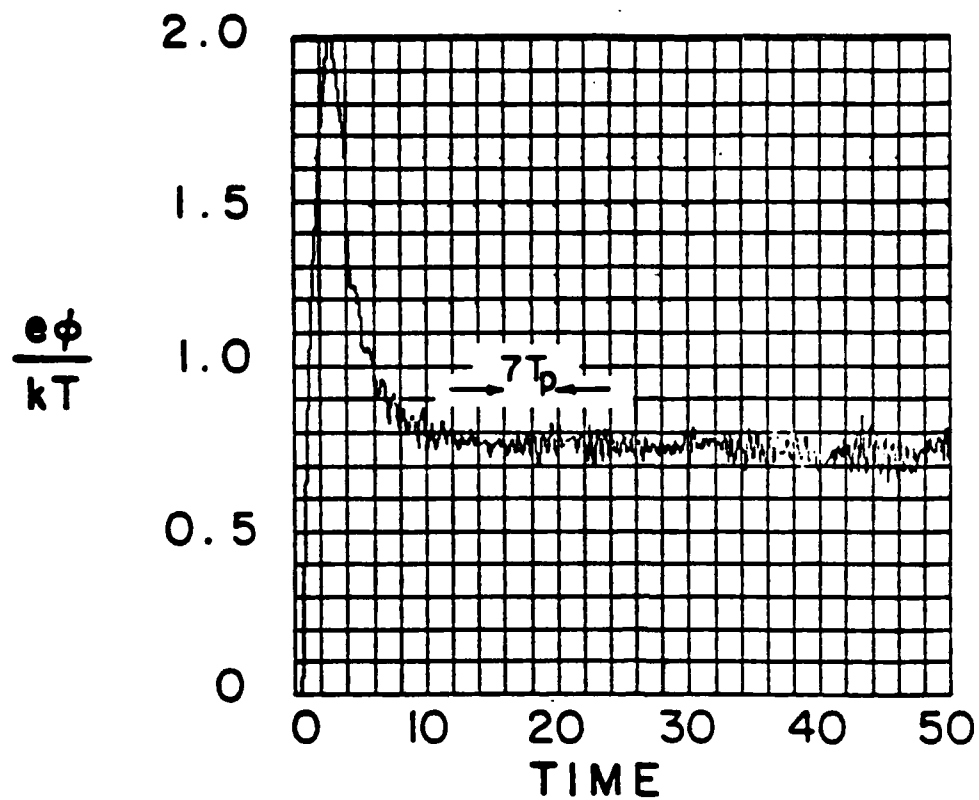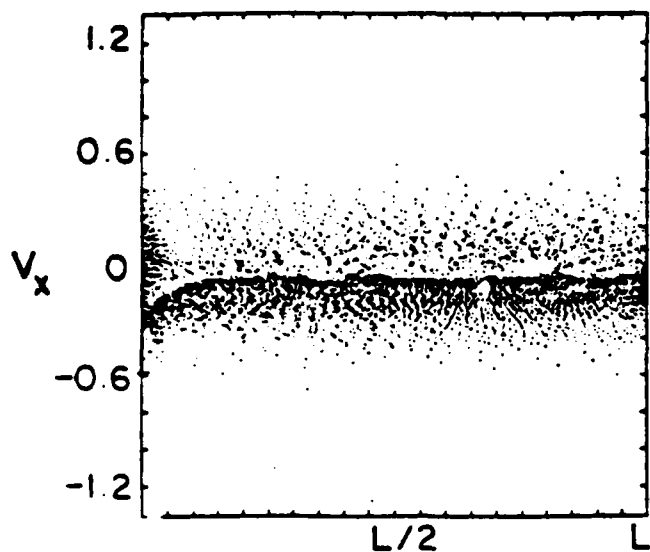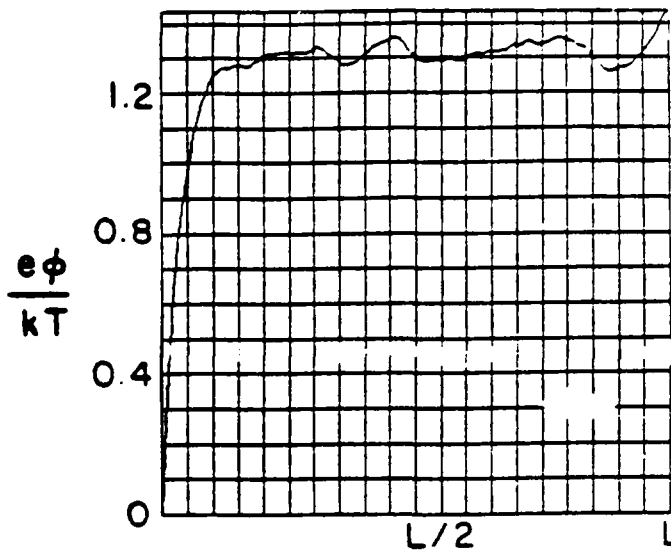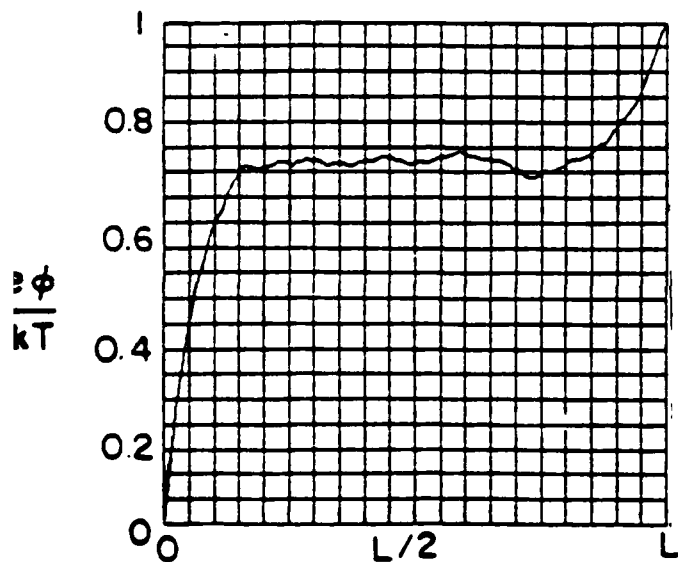
Figure 1. Plasma Model

Figure 2. Electric potential history with
time in step number * DT for (a) purely
absorbing plate and (b) 70% ion reflection
at the plate.

(a)

V_x

L/2   L

SYSTEM LENGTH

(b)

$\dfrac{e\phi}{kT}$

L/2   L

SYSTEM LENGTH

(c)

$\dfrac{e\phi}{kT}$

0   L/2   L

SYSTEM LENGTH

Figure 4. Profiles in (a) ion phase space for 70% reflection, (b) electric potential for 70% reflection, and (c) electric potential for 0% reflection. All at the last time step (at equilibrium).

-6-
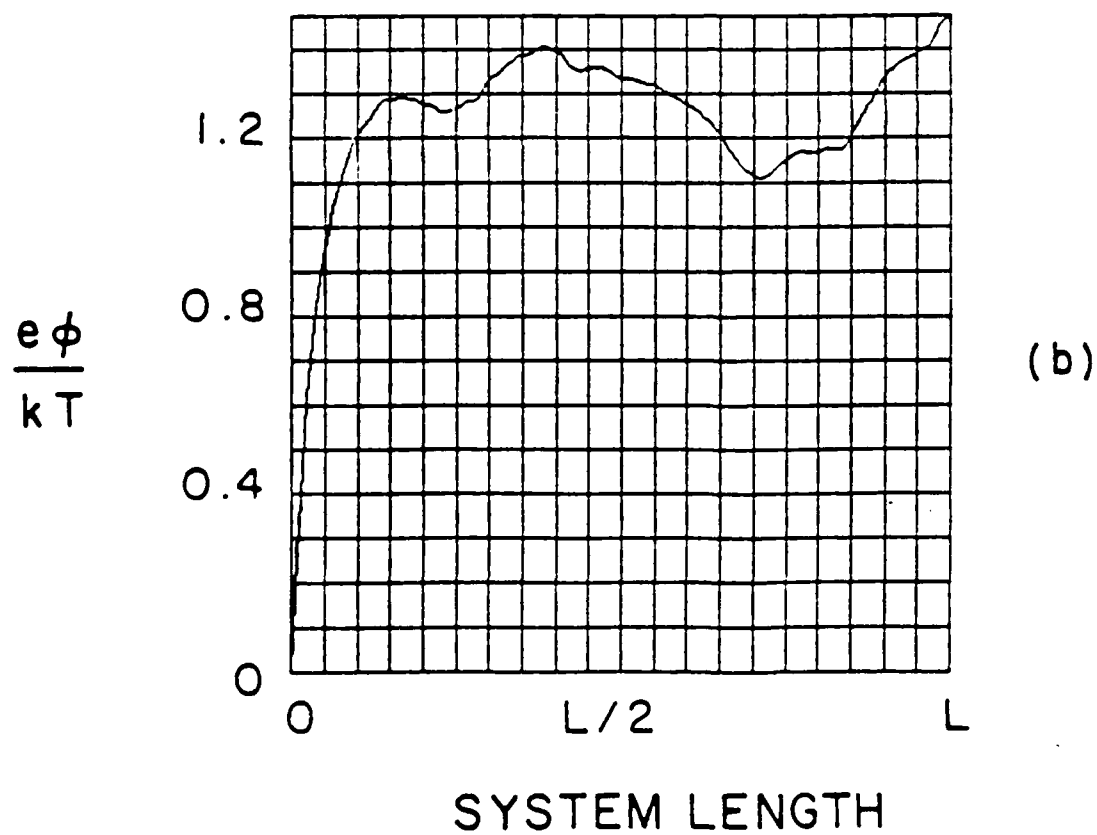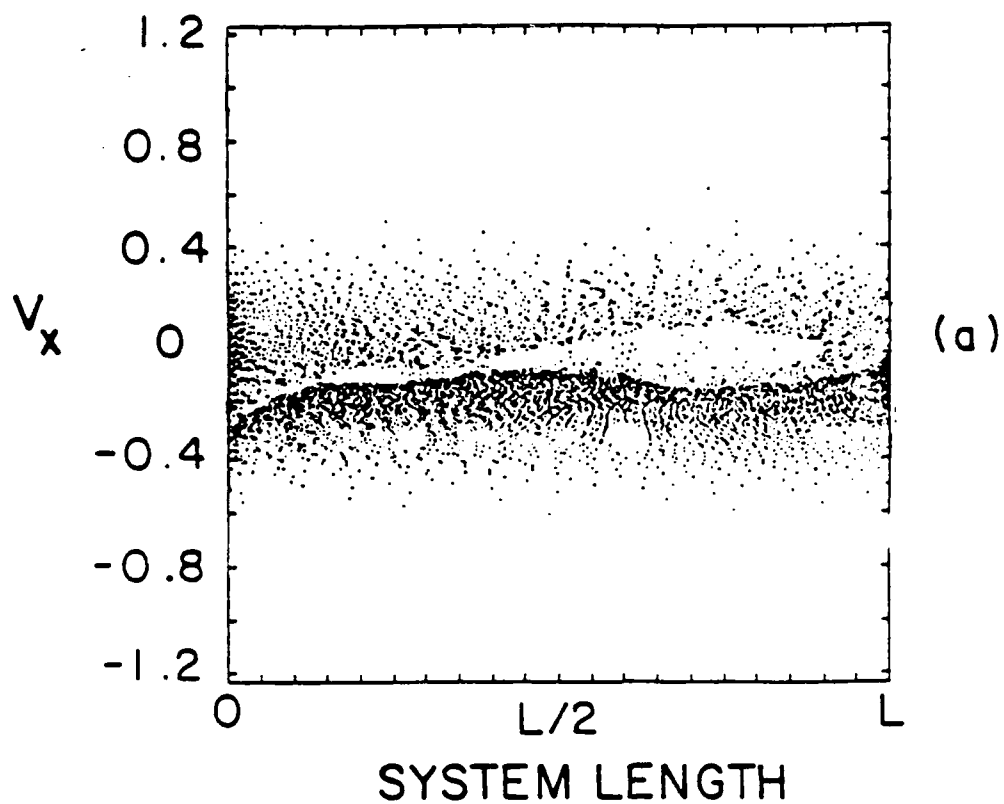
Figure 3. (a) Ion phase space and (b) electric potential profile for 70% wall reflection at time=37.5.
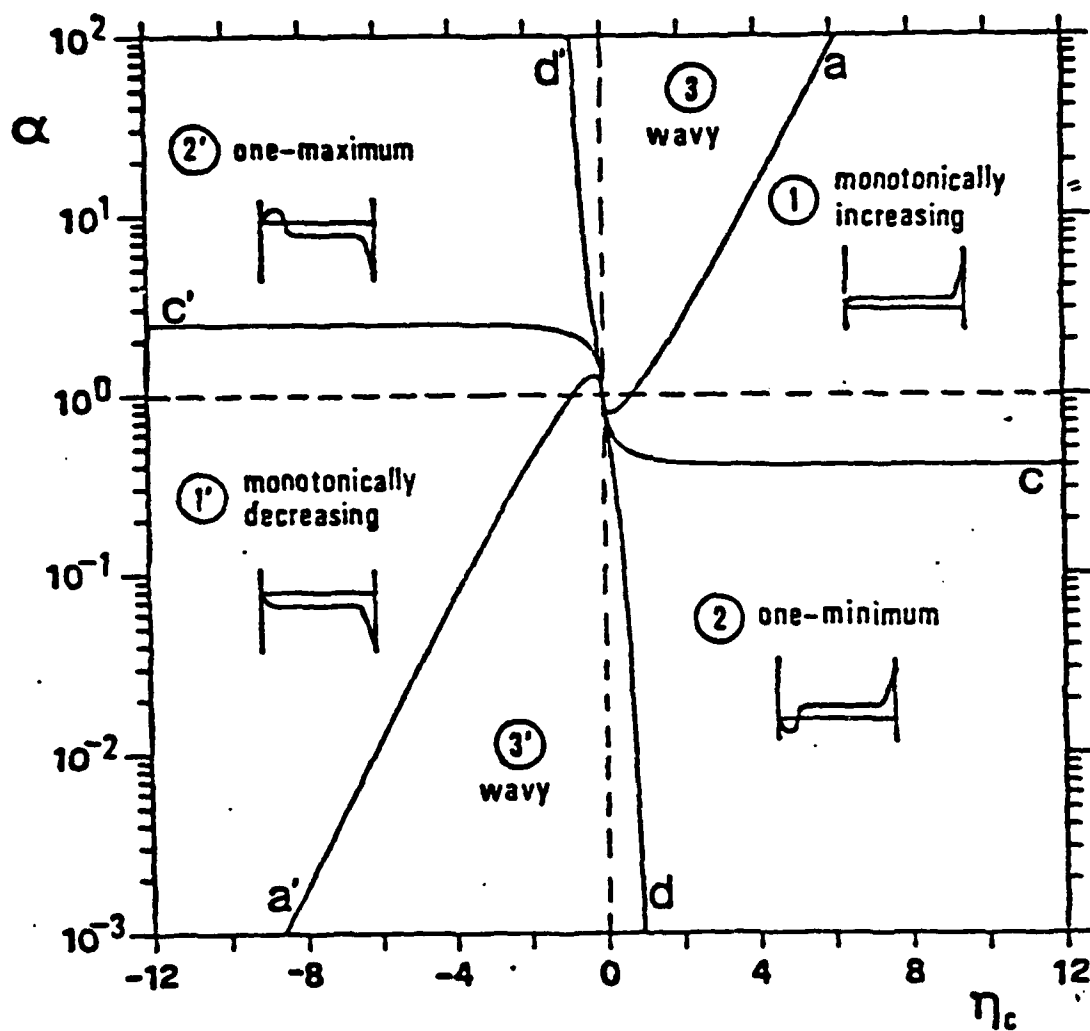
Figure 1., parameter space for the single-ended collisionless Q-machine, α vs. η_{cp}; where $\alpha = n_e^+/n_e^+$ the neutralization parameter, and $\eta_{cp} = e\phi_{cp}/\kappa T$ the normalized wall potential or bias.

$$f_{eo}^+ = exp(-\nu^2) \cdot H(\nu, \eta(x))$$

$$f_{io}^+ = \frac{\alpha}{\sqrt{\mu}} exp(-\frac{\nu^2}{\mu}) \cdot H(\frac{\nu}{\sqrt{\mu}})$$

where $\mu = m_e/M_i$ (and we have normalized to the density of the source electrons, $\frac{2n_i^+}{u_e\sqrt{\pi}}$).

The two parameters α and η_{cp} (the normalized cold plate bias) define the parameter space for the single-ended Q-machine, shown in Figure 1. We are going to consider only the single maximum potential profile, which occurs in the upper left region of parameter space, negative bias with ion rich emission(i.e. $\alpha > 1$). Figure 2 shows the assumed potential profile for the analysis. We now model the distribution functions as functions of potential. For the electrons, for $\eta > 0$ $(x < x_2)$ we have

$$f_e^+(\nu, \eta(x)) = exp\left(-(\nu^2 - \eta(x))\right) \cdot H(\nu - \sqrt{\eta(x)})$$

$$f_e^-(\nu, \eta(x)) = exp\left(-(\nu^2 - \eta(x))\right) \cdot H(\nu + \sqrt{\eta(x)}) \cdot H(\nu - \sqrt{\eta(x) - \eta_{cp}})$$

where we have denoted the positive and negative part of the distribution function by + and − respectively. The low velocity cutoff for f_e^+ is due to the fact that the electrons are initially accelerated by the potential bump as they enter the system from the left. The same is true of the term in f_e^- for the returning, reflected electrons (i.e. in the potential bump the minimum energy a particle should have is $1/2mv^2 = e\phi(x)$). This leads to a 'hole' in electron phase space, which can be seen in Figure 2 where we have drawn

distribution characterized by the temperature of the hot plate. The electrons follow the Richardson-Dushman equation for thermionic emission, this leads to equal electron and ion temperatures ($T_i = T_e = T_{hotplate}$). We then model the distribution for each species at the source by,

$$f_s^+(v) = \frac{2n_{so}^+}{v_{ts}\sqrt{\pi}} \exp(-\frac{v^2}{v_{ts}^2}) \cdot H(v)$$

where $v_{ts} = (2kT/m_s)^{1/2}$, and κ is Boltzmann's constant, and s denotes the species (i.e. $s = e, i$), and $H(v)$ is the Heaviside step function. For convenience we now introduce the following normalization,

$$\chi = \frac{x}{\lambda_{De}} \qquad (length)$$

$$\nu = \frac{v}{v_{te}} \qquad (velocity)$$

$$\eta = \frac{e\phi(x)}{\kappa T} \qquad (potential)$$

where $\lambda_{De} = (\kappa T/4\pi n_{eo}e^2)^{1/2}$ is the Debye length associated with the electron density of the source, and define the neutralization parameter 'α' as,

$$\alpha = \frac{n_{io}^+}{n_{eo}^+}$$

the ratio of the ion to the electron density leaving the source.

We may now write the distribution functions for the source ions and electrons in normalized form as

E.   Corrections to Time Independent Q-Machine Equilibria

Perry C. Gray and Thomas L. Crystal

The 'quiet' plasma machine, or Q-machine, has been used extensively in experiments for examination of basic plasma phenomena.[1] Time independent equilibria for the single-ended collisionless Q-machine have been studied analytically by a number of authors, notably MacIntyre,[2] and Kuhn.[3] The basic analytic approach is to assume a steady state potential profile, monotonic increasing/decreasing or single extremum, assume distribution functions for the plasma source, usually half-Maxwellian, then model the distribution functions as functions of the potential. It is then possible, by integration of Poisson's equation, to define a 'pseudo-potential' and obtain equations that allow one to solve for such quantities as the plasma potential, the potential extremum, and the floating potential for the collector (one also gets values for plasma density). For a review of the technique the reader is directed to Tidman and Krall.[4]

In this paper we restrict our attention to the negative biased, single maximum potential profile, since the simulation[5] of this case yielded results at odds with theory. We will describe the analysis for fixed bias, although floating bias is easily handled with minor modification.

The one dimensional model for the single-ended Q-machine is as follows. The source for the plasma is a hot plate, which we will take to be on the left, and distance is measured positive towards the right, and at $x = L_x$ is a cold collector plate; both are absorbing. The ions are generated from neutral gas according to the Langmuir-Saha law, and hence have a half-Maxwellian

During Phase 2, $|J(t)|$ decreases on the average but shows some very pronounced oscillations.

Phase 3 ($e_2 \leq t \leq e_3$; "electron trapping phase"). This phase is characterized by the formation of a trapped electron population near HP (Figs. 6 and 7), which leads to a small negative potential dip at the low-potential edge af the moving double layer already observed in Fig. 5. This event is also indicated by a little dip in $|J(t)|$.

Phase 4 ($e_3 \leq t \leq b$; "trapped-electron phase"). Throughout this phase, the trapped electron population (which surrounds an eccentrically rotating electron hole) persists and remains localized in the region $0 \leq x \leq o.3$ (Figs. 8 and 9). Adjacent to its right we observe a region of fairly uniform and roughly half-Maxwellian electrons ("plasma region"), and a region of significant electron acceleration to the right ("CP sheath region"). During all of Phase 4, the plasma region spreads to the right, while the CP sheath recedes.

The potential profile always exhibits a relative maximum near HP and remains fairly flat in the plasma region, the potential minimum being negative over most of Phase 4 but going positive at $t \simeq i_4$. By that time , all of the old ions have exited the diode to the left, at a speed about ten times their thermal injection velocity.

At $t = b$, the cycle starts all over again.

[1] N. Rynn, Phys. Fluids 5, 643 (1962) and 9, 165 (1966).
[2] N. Sato et al., Phys. Fluids 19, 70 (1976).
[3] R. Schrittwieser, Phys. Lett. 65A, 235 (1978).
[4] P. Michelsen et al., Plasma Phys. 21, 61 (1979).
[5] S. Iizuka et al., Phys. Rev. Lett. 48, 145 (1982).
[6] R. Schrittwieser, Phys. Lett. 95A, 162 (1983).
[7] P. Burger, J. Appl. Phys. 36, 1938 (1965).
[8] W. Ott, Z. Naturforschg. 22a, 1057 (1967).
[9] S. Kuhn, Plasma Phys. 23, 881 (1981).
[10] S. Kuhn et al., Proc. 1984 ICPP, Lausanne, p. 104 (1984).
[11] Q Machine Simulation Film (16 mm), produced by Plasma Theory and Simulation Group, E.R.L., U.C. Berkeley, CA 94720 (1984).
[12] Wm. S. Lawson, PDW1 User's Manual, Memorandum UCB/ERL M84/37, E.R.L., U.C. Berkeley, CA 94720 (1984).

Fig. 6 t = 13.75

Fig. 7 t = 14.38

Fig. 8 t = 15

Fig. 9 t = 19.38
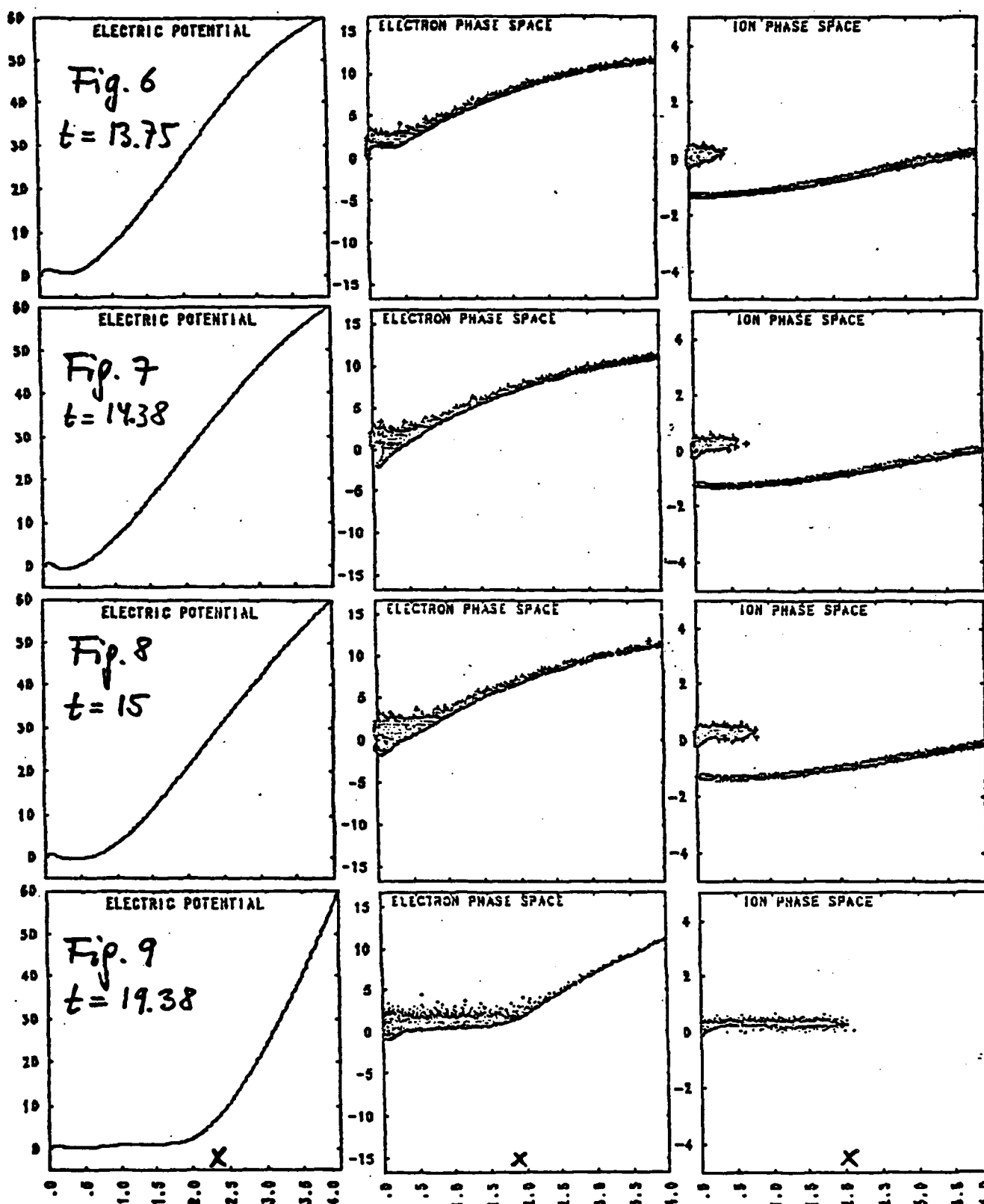
At $t \simeq i_2$ (i.e., approximately at the time the old ions reach CP), the initial monolayer near HP (Fig. 4) turns into a double layer (as indicated by an inflection point in the potential profile, Fig. 5) that starts moving to the right, leaving in its wake a region of low potential.

-16-
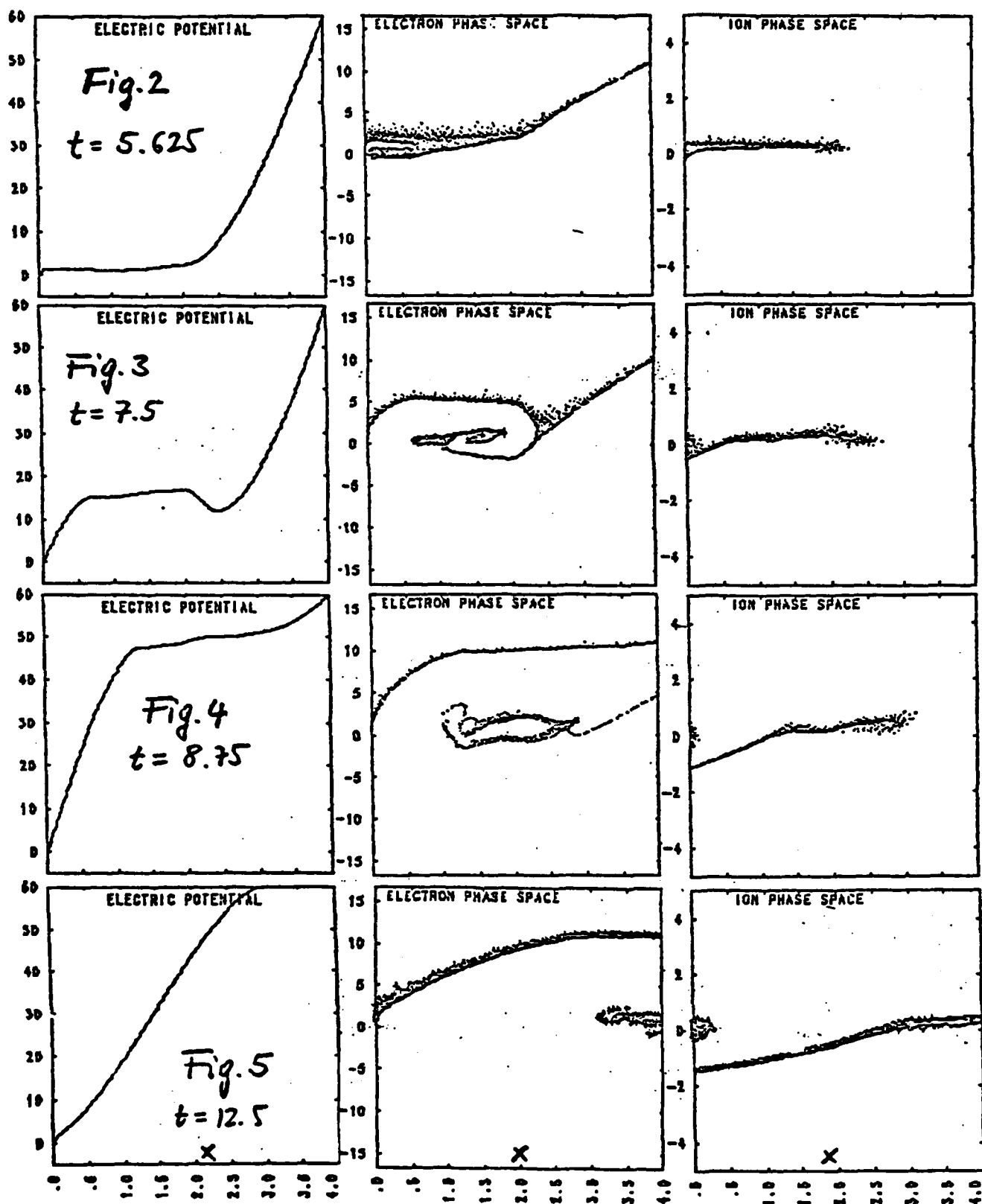
Phase 2 ($e_1 \leq t \leq e_2$; "electron ring phase"). By $t=e_1$, the vortex observed during Phase 1 has closed into what may be loosely called an "electron phase space ring" (Fig. 4). Phase 2 is characterized by the "thermalization" and exiting to the right of this ring (Fig. 5).

Fig. 1
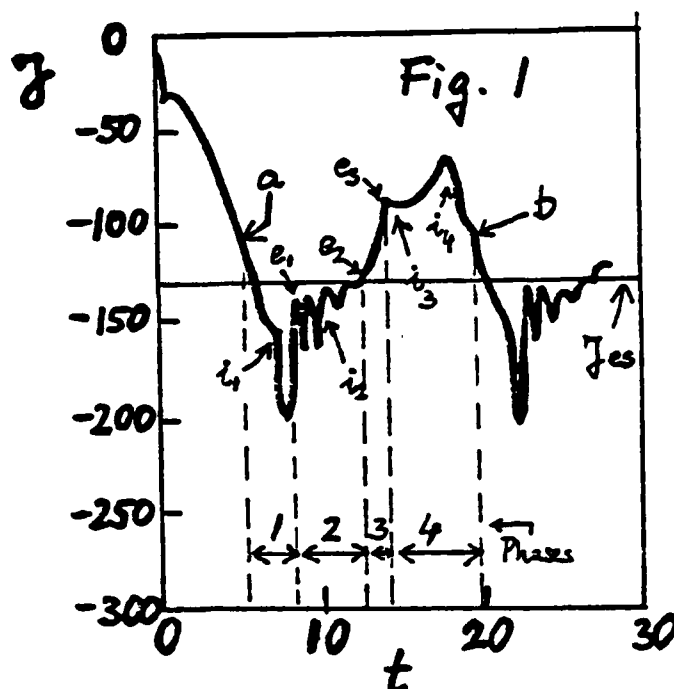
near future.

Close inspection of the simulation data[11] has led us to tentatively subdivide the full cycle into four phases, referred to as Phases 1 through 4 and described below. Each of these phases exhibits a characteristic behavior of electron phase space and also becomes manifest in the external current history. In Fig. 1, times a, e_1, e_2, e_3, and b correspond to characteristic events in electron phase space, while times i_1 through i_4 correspond to characteristic events in ion phase space. The horizontal line marked J_{es} indicates the electron saturation current, i.e., the largest time-averaged current that could possibly be drawn through the diode. For the present run, J_{es} = -127.7.

In what follows, each phase is briefly described and illustrated by two sets of simulation snapshots — one taken at the beginning and the other taken toward the end of the phase in question. Each set contains a potential plot, an electron phase-space plot, and an ion phase-space plot.

<u>Phase 1 ($a \le t \le e_1$; "electron vortex phase")</u>. Conditions right before the onset of Phase 1 are almost identical with those prevailing at the end of Phase 4 (Fig. 9). By definition, Phase 1 commences as the trapped electron population near the hot plate suddenly separates from the "beam" electrons, so as to form a "phase-space vortex" (Fig. 2). Moving to the right, this vortex widens in both x and v, and by the end of Phase 1 evolves into an electron ring.

During the present phase, the space potential flips from low to high, the external current magnitude $|J(t)|$ goes through a sharply peaked maximum, and, at $t=i_1$, the initially coherent ion population splits into the "old" ions (accelerated to the left) and the incoming "new" ions (immediately returned to HP).

-14-

tribute well beyond the present state of understanding of the PRI.

2. <u>MODEL</u>. The model considered is the one-dimensional, collisionless, electrostatic single-emitter plasma diode described, e.g., in Refs. 7-9. Electrons and ions emanate constantly from the hot plate HP (x=0, po-ential V=0, temperature T) with half Maxwellian velocity distributions corresponding to the temperature T and the emission densities n_{eo}^+ and n_{io}^+, respectively. Particles hitting an electrode are absorbed. A constant bias V_C is applied to the cold plate CP (x=L).

The d.c. equilibria of this diode are conveniently classified in terms of the (η_C, α) parameter diagram,[8,9] where $\eta_C = eV_C/kT$ and $\alpha = n_{io}^+/n_{eo}^+$. A quantitative and detailed theoretical study of the four most relevant parameter regions (negative-bias electron-rich, negative-bias ion-rich, positive-bias electron rich, positive-bias ion-rich) was given in Ref. 9, and a preliminary comparison with pertinent particle simulations was presented in Ref. 10. In the meantime, more systematic and detailed simulation data for all four parameter regions have become available in the form of a 16-mm movie,[11] from which the results shown below have been taken. As an example of strongly unstable behavior we have picked out a run whose nondimensional parameters are located in the positive-bias ion-rich region. The simulations were all performed with the new bounded-plasma code PDW1.[12]

3. <u>SIMULATION OF UNSTABLE DIODE BEHAVIOR IN THE POSITIVE-BIAS ION-RICH REGIME</u>. In this section we summarize the results of a simulation run characterized by the nondimensional parameters $\eta_C = 60$, $\alpha = 4$, $\Lambda = 50.6$ (where $\Lambda = L/\sqrt{\varepsilon_0 kT/n_{eo}^+ e^2}$), and $m_i/m_e = 40$. More information concerning this run can be found in Sec. 4a of Ref. 10.

<u>External-current history</u>. Fig. 1 shows the external-circuit current J(t) for the initial transient (fill-up phase) and the first 1.5 cycles of the final dynamic state, which is strictly periodic with period $\Delta t = 14.4$. In what follows, we do not consider the initial transient but rather concentrate on the cyclic behavior. Moreover, the present account is essentially descriptive; our results are still in the stage of discussion, and a more in-depth analysis will hopefully be available in the

D.   Single Ended Plasma Device, Unstable States[*]
PARTICLE SIMULATIONS OF THE UNSTABLE STATES OF A COLLISIONLESS SINGLE-ENDED PLASMA DEVICE

P.L. Gray, S. Kuhn,[**] T.L. Crystal, and C.K. Birdsall

Electronics Research Laboratory, University of California, Berkeley, CA 94720

ABSTRACT. One-dimensional particle simulations of the collisionless single-emitter plasma diode with a positively biased collector plate are reported for "ion-rich" operation. The simulations qualitatively recover several important features of the "potential relaxation instability" observed experimentally, including "moving double layers" followed by a current-limiting potential dip. In addition, the simulation results provide very detailed insight into the electron and ion phase-space dynamics, which can be correlated with the external-current history.

1. INTRODUCTION. It has long been known from both experiments[1-6] and simulations[7] that a low-density single-ended plasma device (such as Q-machine or thermionic converter) may exhibit a large-amplitude, low-frequency longitudinal instability when the cold plate is biased positively with respect to the hot plate. For some time, this instability was believed to be of the "standing ion-acoustic wave" type,[3,4] but more recent experiments with improved potential diagnostics have revealed a much more complex dynamic behavior, including periodic relaxation from a state of high space potential to one of low space potential, via a "moving double layer" followed by a current-limiting potential dip.[5] Accordingly, the phenomenon in question is now quite commonly referred to as "potential relaxation instability (PRI)".[5,6]

In the past, both experiments and simulations have primarily concentrated on establishing the potential profiles and/or carrier density distributions associated with the PRI. To our knowledge, however, no detailed investigation into the related electron and ion phase-space behavior has been reported to date, and it is mainly this aspect where we believe our work to con-

Fig. 6

Fig. 7
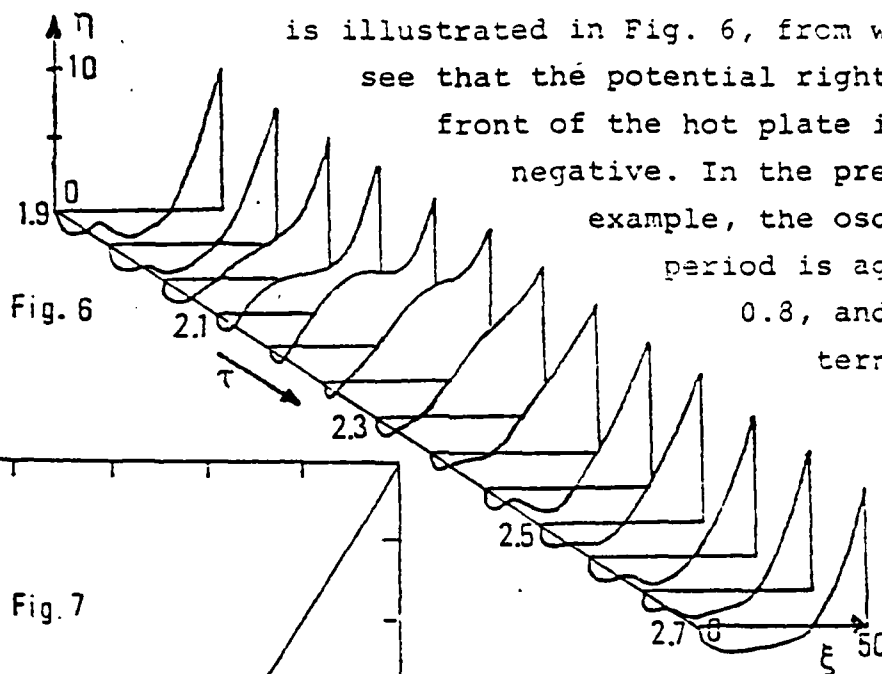
is illustrated in Fig. 6, from which we see that the potential right in front of the hot plate is now negative. In the present example, the oscillation period is again $\Delta\tau = 0.8$, and the external current fluctuates by about 70%.
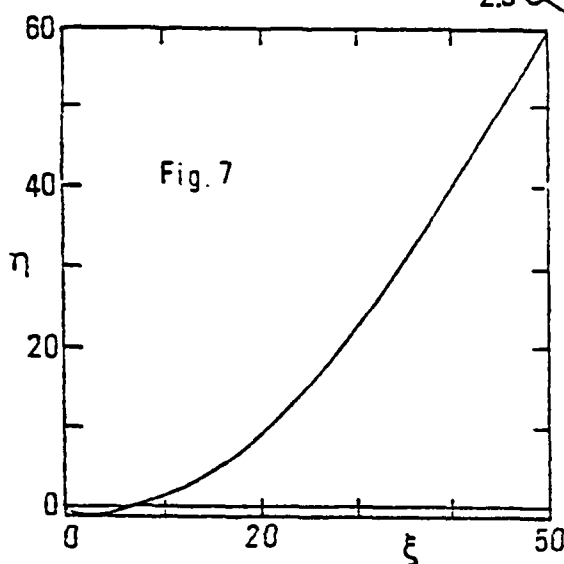
5b. <u>Region 2, parameter point $(\eta_C=60, \alpha=0.1)$</u>. Here too we recover the high-bias stabilization already encountered in Fig. 5 and Ref. 3. The resulting d.c. profile (Fig. 7) exhibits the one-minimum shape expected. However, the quantitative predictions in Ref. 1 are only valid for a diode with a significant quasi-neutral plasma region and hence are not applicable to the "short" diode considered here.

+)Permanent address: Institute for Theoretical Physics, University of Innsbruck, A-6020 Innsbruck, Austria.

1S. Kuhn, Plasma Phys. <u>23</u>, 881 (1981).

2S. Iizuka et al., Phys. Rev. Lett. <u>48</u>, 145 (1982).

3G. Popa et al., Phys. Lett. <u>87A</u>, 175 (1982).

4Wm.S. Lawson, User's Manual for the PDW1 Code, EECS/ERL, U.C. Berkeley, CA 94720 (1984).
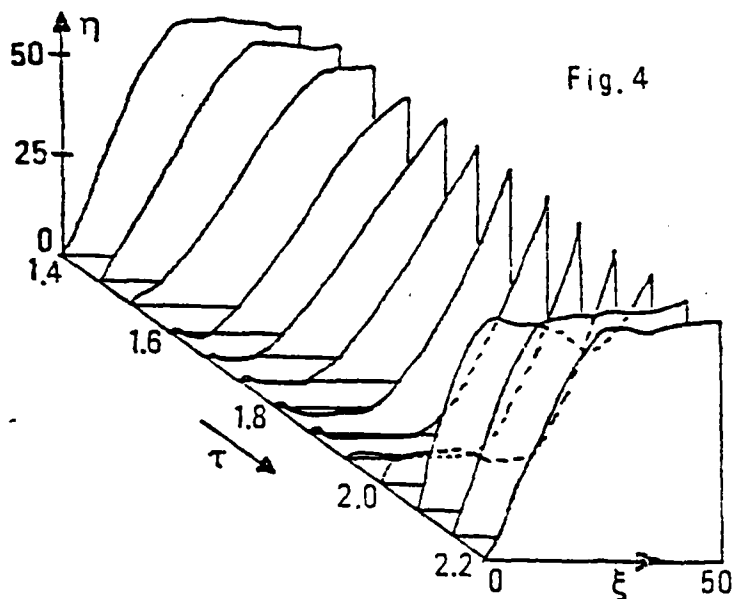
Fig. 4

observed experimentally in Ref. 2. The period is $\Delta\tau \approx 0.8$, and the fluctuation level (defined as peak-to-peak difference over average value) is about 100%. The evolution of the potential profile during one cycle of oscillation (Fig. 4) is qualitatively similar to the one shown in Fig. 1b of Ref. 2. In particular, a negative potential barrier limiting the (electron) current builds up during part of the cycle. Note that the potential always goes positive right in front of the hot plate.

4b. **Region 1, parameter point** $(n_c=150, \alpha=4)$. With the cold-plate bias this high, the large-amplitude oscillations are no longer present, and the diode exhibits an almost time-independent monotonically increasing potential as shown in Fig. 5. This effect of "high-bias stabilization" has also been observed experimentally.[3] In the present example, there are no ions for $\xi \gtrsim 10$, and the system does not develop a quasi-neutral plasma region. Still, the "plasma" properties predicted in Ref. 1
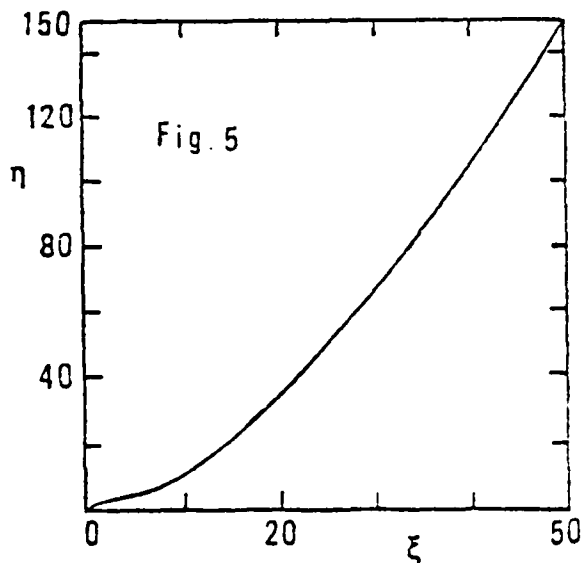
Fig. 5

are relevant in that they apply to the inflection point of the potential profile. E.g., the inflection-point potential predicted is $n_p^{th}=3.37$, in good agreement with Fig. 5.

5a. **Region 2, parameter point** $(n_c=10, \alpha=0.1)$. Again we observe coherent, large-amplitude oscillations similar to those of Fig. 4 and Ref. 2. The time evolution of the potential profile

-10-

PDW1,[4] assuming a mass ratio $m_i/m_e=40$. In each run the diode started out empty, went through a "fillup" phase, and eventually settled down at its "final" state. The results presented below are all related to the respective final states. Potential profiles are displayed in the form[1] $\eta = eV/kT$ vs. $\xi = x/\sqrt{\varepsilon_0 kT/n_{eo}^+ e^2}$, and time is normalized to the ion transit time: $\tau = t\sqrt{2kT/m_i}/L$.

2. _Region 1', parameter point ($n_c=-8,\alpha=0.1$)_. The final state is practically time-independent and exhibits the monotonically decreasing potential profile expected (Fig. 2), the plasma potential being in remarkable agreement with the theoretically predicted value[1] of $n_p^{th} = -4.40$.

Fig. 2
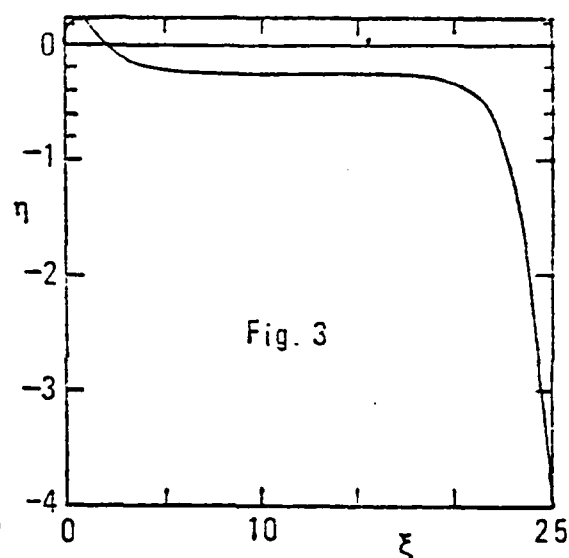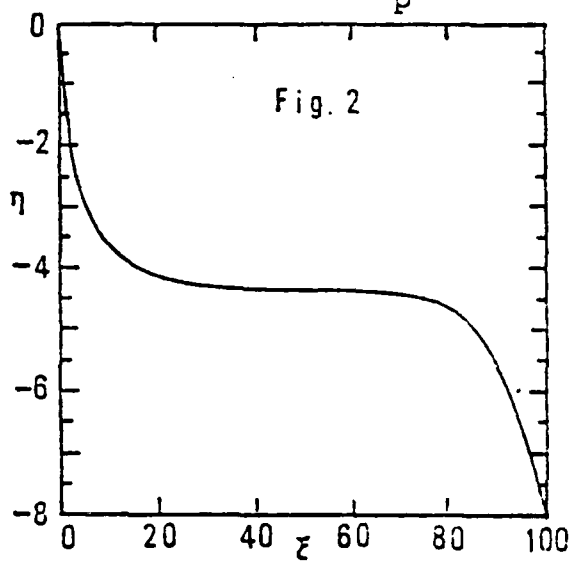
Fig. 3

3. _Region 2', parameter point ($n_c=-4,\alpha=4$)_. In its final state, the diode is again stable, exhibiting a one-maximum profile as predicted (Fig. 3). However, the simulation profile has a maximum potential $n_m^S = 0.25$ and a plasma potential $n_p^S = -0.23$, which values differ significantly from the respective theoretical ones, $n_m^{th}= 0.43$ and $n_p^{th}= -0.60$. This quantitative disagreement has been found to be due to the existence of a trapped electron population in the region of the potential maximum, which originates from the more or less turbulent fillup phase and is not accounted for in Ref. 1.

4a. _Region 1, parameter point ($n_c=60,\alpha=4$)_. In this case, the final state is characterized by coherent large-amplitude oscillations similar to the "potential-relaxation instability"

C.   Single Ended Plasma Device, General Behavior dc and ac[*]

ONE-DIMENSIONAL PARTICLE SIMULATIONS OF THE
COLLISIONLESS SINGLE-ENDED Q MACHINE[*])

S. Kuhn[+]), C.K. Birdsall, T.L. Crystal, P.L. Gray, Wm.S. Lawson

Plasma Theory and Simulation Group, EECS/ERL
University of California, Berkeley, CA 94720

Abstract. Particle simulations of longitudinal phenomena in
the collisionless single-ended Q machine recover some bas-
ic equilibrium properties predicted theoretically, as well as
the "potential-relaxation instability" and its "high-bias sta-
bilization" observed experimentally. The results provide a
starting point for more detailed investigations in various
directions.

1. Introduction. The model considered is the one-dimensional,
collisionless, electrostatic single-emitter plasma diode de-
scribed, e.g., in Ref. 1. Electrons and ions emanate constant-
ly from the hot plate (x=0, potential V=0, temperature T) with
half Maxwellian velocity distributions corresponding to the
temperature T and the emission densities n_{eo}^{+} and n_{io}^{+}, respec-
tively. Particles hitting an electrode are absorbed. A con-
stant bias V_c is applied to the cold plate (x=L).

In Ref. 1, the d.c. equilibria of this diode were studied
with the assumption that there are no trapped particles in the
potential wells. They were classified in terms of the (η_c, α)
parameter diagram shown in Fig.
1, where $\eta_c = eV_c/kT$ and $\alpha = n_{io}^{+}/n_{eo}^{+}$.
In the present paper, we describe
simulation runs for four param-
eter points (η_c, α) representa-
tive of the parameter regions
1', 2', 1, and 2. The results
are compared with predictions
of Ref. 1 and recent experiment-
al observations.[2,3]
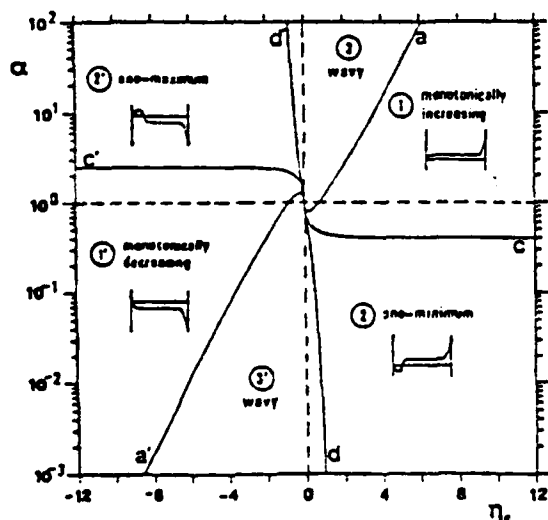
The simulations were performed
with the new bounded-plasma code

Fig.1 D.c. potential profiles

-8-
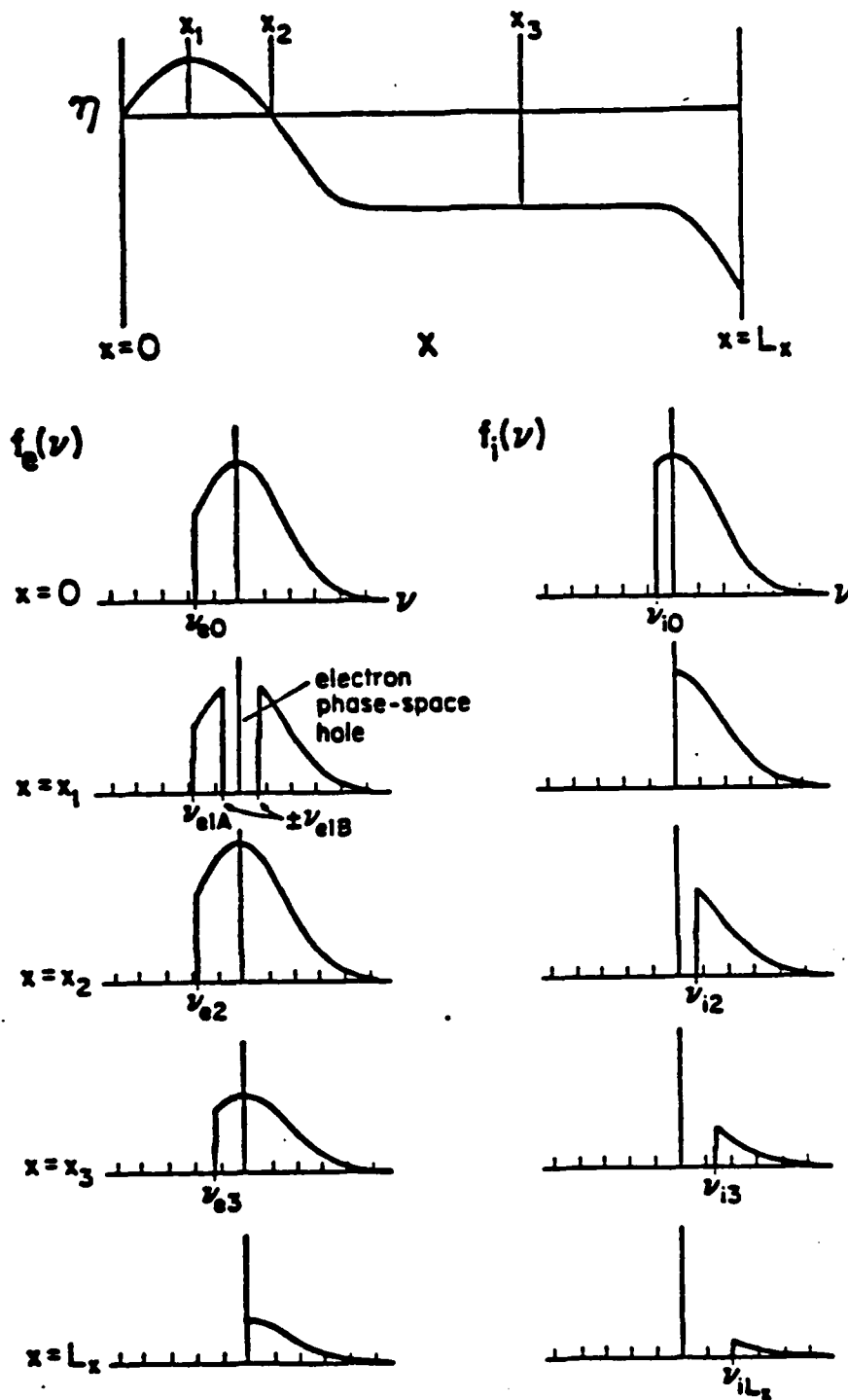
Figure 2., the assumed potential profile for single-maximum case, and electron and ion distribution functions at various positions along the profile; for electrons $\nu_{eo} = -\sqrt{-\eta_{cp}}$, $\nu_{e1a} = -\sqrt{\eta_{max} - \eta_{cp}}$, $\nu_{e1b} = \pm\sqrt{\eta_{max}}$, $\nu_{e2} = -\sqrt{-\eta_{cp}}$, $\nu_{e3} = -\sqrt{\eta_p - \eta_{cp}}$; for ions $\mu = m_e/M_i$, $\nu_{io} = -\sqrt{\mu\eta_{max}}$, $\nu_{i2} = \sqrt{\mu\eta_{max}}$, $\nu_{i3} = \sqrt{-\mu\eta_p}$, $\nu_{iL_x} = \sqrt{-\mu\eta_{cp}}$.

the distribution functions for the two species at different positions along the potential profile, as indicated. The high velocity cutoff in f_e^- merely reflects the fact that electrons with initial energy greater than $e\phi_{cp}$ make it across the system and impinge on the collector plate (i.e. the negative half of the distribution is due entirely to reflected electrons). For $\eta < 0$ ($x > x_2$), we have for the electron distribution function,

$$f_e(\nu, \eta(\chi)) = \exp\Big(-(\nu_2 - \eta(\chi))\Big) \cdot H(\nu + \sqrt{\eta(\chi) - \eta_{cp}}).$$

where again the high negative velocity cutoff indicates the electron with enough energy to reach the cold plate.

For the ion distribution function we have, for $x < x_1$

$$f_i(\nu, \eta(\chi)) = \alpha \exp\Big(-(\frac{\nu^2}{\mu} + \eta(\chi))\Big) \cdot H(\frac{\nu}{\sqrt{\mu}} + \sqrt{\eta_{max} - \eta}).$$

The incoming ions are initially slowed by the potential bump and those with energy less than $e\phi_{max}$ are reflected. For $x > x_1$ we have,

$$f_i(\nu, \eta(\chi)) = \alpha \exp\Big(-(\frac{\nu^2}{\mu} + \eta(\chi))\Big) \cdot H(\frac{\nu}{\sqrt{\mu}} - \sqrt{\eta_{max} - \eta})$$

Those ions which are not reflected by the potential bump are accelerated towards the wall.

We would like to obtain a set of equations which will allow us to calculate the potential maximum and the plasma potential, given a choice of α and η_{cp}. The first equation we will obtain from Poisson's equation and the fact that the electric field in the plasma region is zero. We can write Poisson's equation in normalized quantities as

$$\frac{\partial^2 \eta}{\partial \chi^2} = n_e(\chi, \eta) - n_i(\chi, \eta) \equiv \frac{\partial \psi}{\partial \eta}$$

-23-

the quantity ψ is often referred to as the Sagdeev-potential or pseudo-potential, and is proportional to the square of the electric field. Multiplying this by $\partial\eta/\partial\chi$ and integrating with respect to χ we get

$$1/2\left(\frac{\partial\eta}{\partial\chi}\right)^2 - \psi + C = 0$$

where C is an arbitary constant. We know that

$$\left.\frac{\partial\eta}{\partial\chi}\right|_{\chi=\chi_1} = \left.\frac{\partial\eta}{\partial\chi}\right|_{\chi=\chi_3} = 0$$

so that

$$\psi(\eta_{max}) = \psi(\eta_p).$$

Integrating the expressions for n_i and n_e with respect to potential from $\eta = \eta_{max}$ to $\eta = \eta_p$, we obtain the first relation

$$
\begin{aligned}
\psi(\eta_p) - \psi(\eta_{max}) = &\exp(\eta_p)\left(1 + \mathrm{erf}\sqrt{\eta_p - \eta_{cp}}\right) \\
&- \exp(\eta_{max})\left(1 + \mathrm{erf}\sqrt{\eta_{max} - \eta_{cp}}\right) \\
&+ \frac{2}{\sqrt{\pi}}\exp(\eta_{cp})\left(\sqrt{\eta_{max} - \eta_{cp}} - \sqrt{\eta_p - \eta_{cp}}\right) \\
&+ 2\left(\exp(\eta_{max})\mathrm{erf}\sqrt{\eta_{max}} - \frac{2}{\sqrt{\pi}}\sqrt{\eta}_{max}\right) \\
&+ \alpha\exp(-\eta_p)\left(1 - \mathrm{erf}\sqrt{\eta_{max} - \eta_p}\right) \\
&- \alpha\exp(-\eta_{max})\left(1 - \frac{2}{\sqrt{\pi}}\sqrt{\eta_{max} - \eta_p}\right) = 0.
\end{aligned}
$$

where $\mathrm{erf}(x) \equiv \frac{2}{\sqrt{\pi}}\int_0^x exp(-y^2)dy$. The fourth term in the expression above is due to the assumed presence of the hole in electron phase space.

-24-

The second relation comes from the quasi-neutrality condition in the plasma region $\left(n_i(\eta_p) = n_e(\eta_p)\right)$. By integrating the distribution functions over velocity we get

$$\exp(\eta_p)\left(1 + \mathrm{erf}\sqrt{\eta_p - \eta_{cp}}\right) - \alpha\,\exp(-\eta_p)\left(1 - \mathrm{erf}\sqrt{\eta_{max} - \eta_p}\right) = 0.$$

These two equations will allow us to determine η_{max} and η_p given initial choices of α and cold plate bias η_{cp}. For the case of a floating cold plate the additional equation required is supplied by the condition that the electron and ion fluxes to the cold plate must be equal at equilibrium.

From our simulation study of equilibria in the single-ended Q-machine we have found that the 'hole' in electron phase space, for single maximum potential profiles, is filled to a Maxwell-Boltzmann level. This can be seen from Figure 3 which shows the potential profile for a typical simulation for such a case, as well as the time average distribution function for the electrons windowed across the potential bump as indicated. We have also plotted the expected Maxwell-Boltzmann distribution on top of the simulation result for comparison. Assuming this to be the case simplifies the model for the electron distribution function, which becomes

$$f_e(\nu, \eta(x)) = \exp\left(-(\nu^2 - \eta(x))\right)\,\cdot\,H(\nu + \sqrt{\eta(x) - \eta_{cp}}).$$

Having assumed that the electron phase space hole is filled, the first of the two relations above becomes

-25-
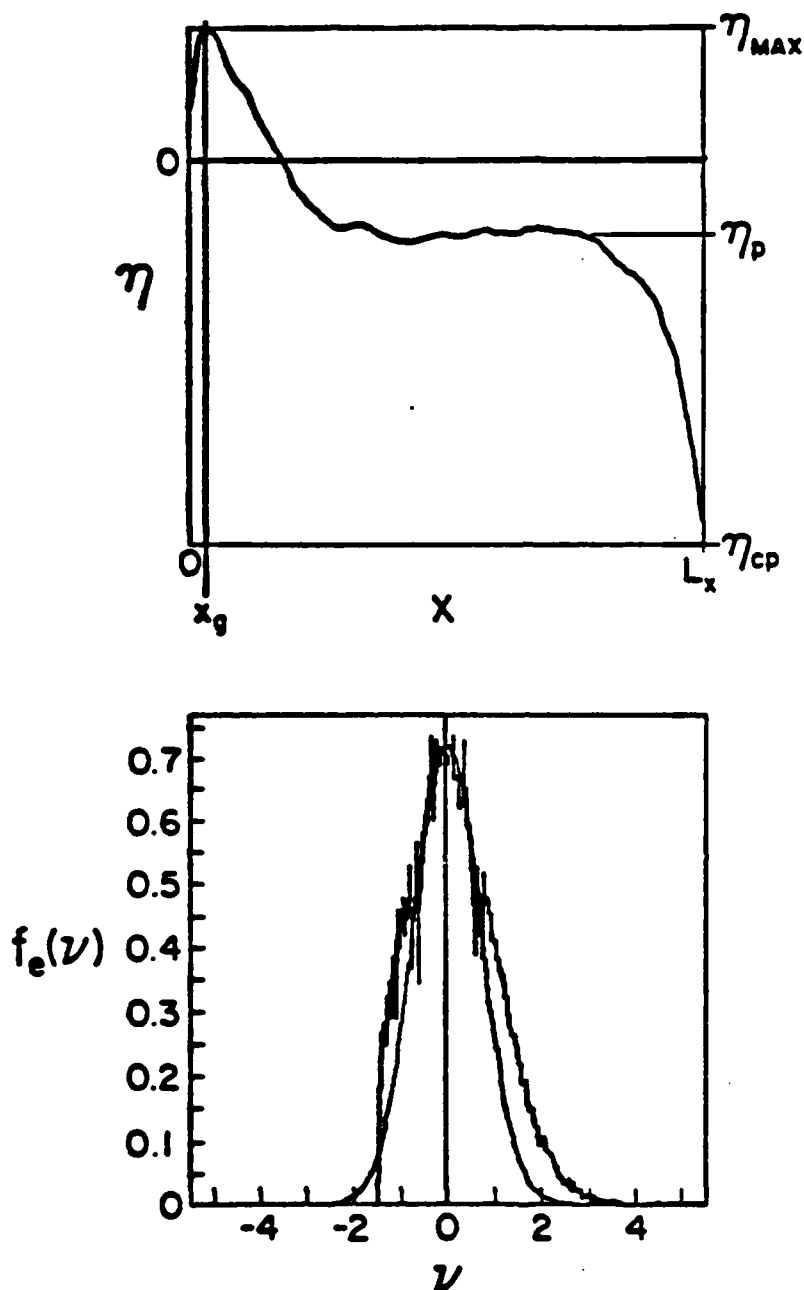
Figure 3., the single-maximum potential profile from a simulation with
$a = 4.0$ and $\eta_{cp} = floating$(ie. $\approx$ −1.84), and the time averaged electron
distribution function calculated at $\chi = \chi_g$ as indicated on the potential
profile.

$$\psi(\eta_p) - \psi(\eta_{max}) = \exp(\eta_p)\left(1 + \operatorname{erf}\sqrt{\eta_p - \eta_{cp}}\right)$$

$$- \exp(\eta_{max})\left(1 + \operatorname{erf}\sqrt{\eta_{max} - \eta_{cp}}\right)$$

$$+ \frac{2}{\sqrt{\pi}}\exp(\eta_{cp})\left(\sqrt{\eta_{max} - \eta_{cp}} - \sqrt{\eta_p - \eta_{cp}}\right)$$

$$+ \alpha\exp(-\eta_p)\left(1 - \operatorname{erf}\sqrt{\eta_{max} - \eta_p}\right)$$

$$- \alpha\exp(-\eta_{max})\left(1 - \frac{2}{\sqrt{\pi}}\sqrt{\eta_{max} - \eta_p}\right) = 0.$$

it differs from the realation for the initial model only in the abscence of the term for the phase space hole.

Figures 4 and 5 show the comparison of simulation results with the numerical calculation of the predicted values for η_p and η_{max} for a cold plate bias of $\eta_{cp} = -4.0$, as functions of neutralization parameter α. As can be seen the calculation with the assumption of the electron phase space hole being filled to a Maxwell-Boltzmann level agrees very well with the results from our simulation study.

The fact that the electron phase space hole fills to a Maxwell-Boltzmann level is as yet unexplained. We believe it is due to trapping of electrons by fluctuation of the potential profile. In reasonably long simulations with $\alpha = 4.0$ and a floating cold plate, we have observed the trapinng vortex to expand into the system while maintaining the potential extremum predicted by the above analysis. This might lead one to think that there might exist an extremely long period relaxation process as has been observed in other simulations.[5]. We are currently examining this posibility.
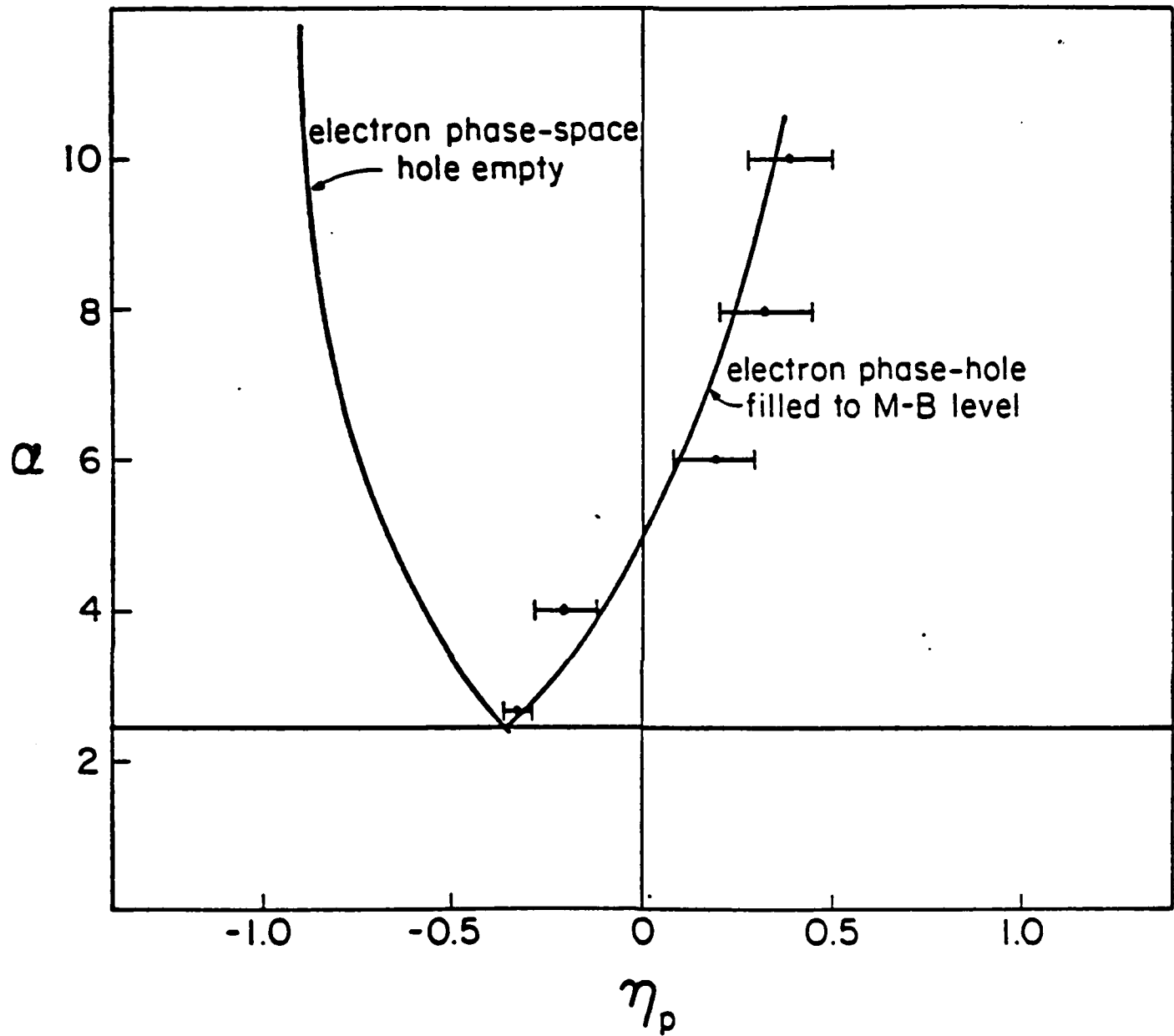
Figure 4., η_p vs. α from numerical calculations assuming the electron phase-space hole to be filled, empty, and results from simulations.

Figure 5. η_{max} vs. α from numerical calculations assuming the electron phase-space hole to be filled, empty, and resultes from simulations.

References

[1]Motley, R. W., *Q-Machines*, Academic Press, New York, 1975.

[2]McIntyre, R. G., *"Extended Space-Charge Theory in Low-Pressure Thermionic Converters"*, Journal of Applied Physics, Vol. 33, No. 8, 1962.

[3]Kuhn, S., *"Axial Equilibria, Disruptive Effects, and Buneman Instability in Collisionless Single-Ended Q-Machines"*, Plasma Physics, Vol. 23, No. 10, pp. 881-902, 1981.

[4]Tidman, D. A. and N. A. Krall, *Shock Waves in Collisionless Plasma*, J. Wiley, N. Y., 1971.

[5]Gray, P. C., S. Kuhn, T. L. Crystal, and C. K. Birdsall, it *"Particle Simulations of the Unstable States of a Collisionless Single-Ended Plasma Device"*, Proc. Second Symposium on Plasma Double Layers and Related Topics, Innsbruck Austria, July 1984.

F. MULTIFLUID DERIVATION OF THE ALFVÉN ION-CYCLOTRON LINEAR DISPERSION RELATION

Niels F. Otani (Prof. C. K. Birdsall)

The linear dispersion relation appropriate to the Alfvén ion-cyclotron (AIC) instability is well-known for propagation of the wave along the background magnetic field B_0 in a uniform plasma (e.g., see Ref. 1). Here we again derive the AIC dispersion relation but use a "multifluid" model instead of the more usual Vlasov equation as the basis for the calculation. The advantage of this approach lies in its conceptual simplicity—one observes the direct connection between features of the wave responsible for producing the various linear currents and terms in the dispersion relation.

Assume for the moment an unperturbed ion distribution of the form

$$f_i^0(v_z, v_\perp, \theta) = f^0(v_z, v_\perp)p^0(\theta)$$

with the normalizations

$$\int dv_z dv_\perp f^0(v_z, v_\perp) = 1$$

$$\int_0^{2\pi} d\theta p^0(\theta) = 1.$$

The distribution function is thus uniform in space and separable with respect to the gyrophase angle θ. It is not, however, time-independent, since θ is not a zero-order constant of the motion.

By considering the ion phase space fluid in the Vlasov description to be composed of an uncountably infinite number of cold fluids, each with its own characteristic set of zero-order quantities v_z, $v_\perp$, and θ at time t, we may write the perturbed ion current in, say, the $\hat{y}$-direction as

$$(J_i)_{y1}(z,t) = e \int dv_z dv_\perp f^0(v_z, v_\perp) \int d\theta p^0(\theta)(n_0 v_{y1}(v_z, z, t) + n_1(v_z, v_\perp, \theta, z, t)v_y) \quad (1)$$

In this expression n_0 is the unperturbed ion density, $v_y = v_\perp \cos\theta$, and $v_{y1}(v_z, z, t)$ and $dv_z dv_\perp f_0 n_1(v_z, v_\perp, \theta, z, t)$ are respectively the perturbation $\hat{y}$-velocity and perturbation density of the cold fluid element with zero-order quantities v_z, $v_\perp$, θ, and z at time t. A mathematically rigorous derivation of this infinite fluid model exists and will be presented in a future report.

The perturbation density may be expressed as:

$$n_1(v_z, v_\perp, \theta, z, t) = -n_0 \frac{\partial}{\partial z} z_1(v_z, v_\perp, \theta, z, t)$$

Thus

$$(J_i)_{y1} = n_0 e \int dv_z dv_\perp f^0(v_z, v_\perp) \int d\theta p^0(\theta)(v_{y1}(v_z, z, t) - v_y \frac{\partial}{\partial z} z_1(v_z, v_\perp, \theta, z, t)). \quad (2)$$

Now consider the motion of ions in a single, purely transverse, circularly polarized, sinusoidal wave of wavenumber k and frequency ω propagating in the direction of a uniform magnetic field $\mathbf{B_0}$. The fields are described by

$$\mathbf{B}(z,t) = B_0\hat{z} + B_1(-\hat{x}\sin(kz - \omega t) + \hat{y}\cos(kz - \omega t))$$

$$\mathbf{E}(z,t) = \frac{\omega B_1}{kc}(\hat{x}\cos(kz - \omega t) + \hat{y}\sin(kz - \omega t)).$$

The ion equations of motion in rectangular coordinates are

$$\frac{d\mathbf{v}}{dt} = \frac{e}{m}\left(\mathbf{E}(z,t) + \frac{\mathbf{v} \times \mathbf{B}(z,t)}{c}\right) \tag{3}$$

where m is the ion mass.

Linearized ion orbits may be derived from Eq. (3) given the zero-order orbits

$$v_{x0}(t) = v_{\perp 0}\sin(\Omega t + \theta_0)$$

$$v_{y0}(t) = v_{\perp 0}\cos(\Omega t + \theta_0)$$

$$z_0(t) = z_0 + v_{z0}t$$

where $\Omega \equiv \omega_{ci} \equiv eB_0/mc$. We obtain for small wave perturbations, (real part implied):

$$v_{x1}(t) = \frac{i}{k}\frac{eB_1}{mc}\frac{\omega - kv_{z0}}{\omega - kv_{z0} - \Omega}\exp(ikz_0(t) - i\omega t) \tag{4}$$

$$v_{y1}(t) = \frac{eB_1}{kmc}\frac{\omega - kv_{z0}}{\omega - kv_{z0} - \Omega}\exp(ikz_0(t) - i\omega t) \tag{5}$$

$$v_{z1}(t) = \frac{eB_1/mc}{-i(\omega - kv_{z0} - \Omega)}(v_{x0}(t) - iv_{y0}(t))\exp(ikz_0(t) - i\omega t) \tag{6}$$

$$z_1(t) = -\frac{eB_1/mc}{(\omega - kv_{z0} - \Omega)^2}(v_{x0}(t) - iv_{y0}(t))\exp(ikz_0(t) - i\omega t). \tag{7}$$

Substituting these linearized fluid quantities into Eq. (2), we obtain (real part implied):

$$(J_i)_{y1} = \frac{n_0e^2B_1}{kmc}\int dv_z dv_\perp f^0(v_z, v_\perp)\int d\theta p^0(\theta)$$

$$\times \left(\frac{\omega - kv_z}{\omega - kv_z - \Omega} + \frac{k^2v_\perp^2}{(\omega - kv_z - \Omega)^2}\cos\theta(\cos\theta + i\sin\theta)\right)e^{ikz - i\omega t} \tag{8}$$

Here we note that a time-dependent unperturbed distribution function will still yield a perturbed current varying as $e^{ikz - i\omega t}$ provided $\int d\theta p^0(\theta)\cos^2\theta$ and $\int d\theta p^0(\theta)\sin\theta\cos\theta$ are time-independent. This is true in particular for the "four-spokes" distribution functions used in many of our simulations. We now restrict our derivation to distributions with

$$\int d\theta p^0(\theta)\cos^2\theta = \tfrac{1}{2}$$

and

$$\int d\theta p^0(\theta)\sin\theta\cos\theta = 0$$

which is true of both four-spokes distributions and gyrophase-independent distributions. Thus,

$$\frac{4\pi(J_i)_{y1}}{c} = \frac{B_1}{k}\frac{\Omega^2}{v_A^2}\int dv_z dv_\perp f^0(v_z,v_\perp)\left(\frac{\omega - kv_z}{\omega - kv_z - \Omega} + \frac{\frac{1}{2}k^2v_\perp^2}{(\omega - kv_z - \Omega)^2}\right)e^{ikz - i\omega t} \quad (9)$$

The electrons may be assumed to be a cold fluid, drifting in response to the perturbation transverse electric field with the $\mathbf{E}\times\mathbf{B}$ velocity:

$$\frac{4\pi(J_e)_{y1}}{c} = -\frac{4\pi e n_0}{c}\frac{c(\mathbf{E}_1\times\mathbf{B}_0)_y}{B_0^2}$$

$$= \frac{\omega\Omega}{kv_A^2}B_1 e^{ikz - i\omega t}$$

Finally,

$$(\nabla\times\mathbf{B}_1)_y = -kB_1 e^{ikz - i\omega t}.$$

Ampere's Law then yields the AIC dispersion relation:

$$0 = \frac{k^2v_A^2}{\Omega^2} + \frac{\omega}{\Omega} + \int dv_z dv_\perp f^0(v_z,v_\perp)\left(\frac{\omega - kv_z}{\omega - kv_z - \Omega} + \frac{\frac{1}{2}k^2v_\perp^2}{(\omega - kv_z - \Omega)^2}\right) \quad (10)$$

The first term is the free-space term and the second term is the electron $\mathbf{E}\times\mathbf{B}$ contribution. From the infinite fluid derivation, we know the third term comes from the perturbation transverse ion motion, while the fourth term arises from the transverse ion current generated by the inhomogeneous first-order displacements of ions along $\mathbf{B}_0$. The current appears because the different fluids, with different zero-order transverse velocities, experience different differential displacements, and therefore contribute with different densities to the transverse current density at a given location z. It is this last term which is responsible for the AIC instability.

References

[1]R. C. Davidson and J. M. Ogden, "Electromagnetic Ion Cyclotron Instability Driven by Ion Energy Anisotropy in High-Beta Plasmas." Physics of Fluids 18, 1045 (1975).

G.   POTENTIAL BARRIER BETWEEN HOT AND COOL PLASMAS

Seigi Ishiguro, Inst. of Plasma Physics,
Nagoya, Japan (Prof. C. K. Birdsall)

A potential depression is observed between two plasmas with different electron temperature in Q-machine experiment [1]. In order to study this problem, using the PDW1 code, we have performed one dimensional particle simulations with nonperiodic boundary conditions.

The conditions employed inthe simulation are the following: Particles are injected with half Maxwellian distribution from each sidewall and particles which collide with the walls are absorbed. Ion to electron mass ratios are m_i/m_e = 4, 25; ion to electron temperature ratio is T_i/T_e = 1, and hot to cool electron temperature ratio is T_{eh}/T_{ec} = 4. Hot and cool electron thermal velocities are v_{teh} = 1, v_{tec} = 0.5. The injected current density from the hot side for electrons is J_{eh} = 4, the system length is L = 8, the timestep increment DT = 0.02, and number of time step in a run is NT = 6400.

When the system is initially empty, the plasma is turbulent in the early stage, and appears to seek equilibrium. No interface is observed between the hot and cool side. See Figure 1 shows the ion phase space.

When the system is initially full, formation of ion holes is observed as shown in Figure 2, also ion phase space. These ion holes move from the cool side to hot side with v_{hole} ≐ 0.12. This velocity is smaller than C_{sh} ($=v_{teh}\sqrt{\frac{m_e}{m_i}}$ = 0.2) and greater than C_{sc} ($=v_{tec}\sqrt{\frac{m_e}{m_i}}$ = 0.1). [Note the similarity between these holes (please space vortices) and the real space (x,y) vortices between two fluids as formed in the Kelvin Helmholtz

instability, at saturation]. The potential of the plasma and right side wall (floating) oscillates with plasma frequency; with amplitude $e\phi/KT_{hot} \approx 0.2$, modulated at a low frequency (like $\omega_p/20$), as seen in Figures 3 and 4. A spatial interface is not observed as was seen in the laboratory experiments.

Some next step may include:

(a) Using $\phi(x)$ time averaged (over at least τ_{plasma} oscillation) in order to see whether the transient ion holes occur at potential dips;

(b) Loading x,v space close to the $f_0(x,v)$ expected from equilibrium, complete with ion hole and reflected electrons at t = 0.

(c) Imposing the expected $\phi(x)$ for some time $0 < T < T_S$ (no Poisson solver) where T_S is several ion thermal particle transit times, in order to form the ion hole. As $t > T_S$ the imposed $\phi(x)$ may be slowly turned off and the Poisson solver turned on (suggested by N. Otani).

Reference

[1] R. Hatakeyama, Y. Suzuki, N. Sato, "Formation of Electrostatic Potential Barrier Between Different Plasmas," Phys. Rev. Lett. 50, pp. 1203-1206, 18 April 1983.

ONE-DIMENSIONAL PARTICLE SIMULATIONS OF THE
COLLISIONLESS SINGLE-ENDED Q MACHINE[1])

S.Kuhn[2]), C.K. Birdsall, T.L. Crystal, P.L. Gray, Wm.S. Lawson

Plasma Theory and Simulation Group
Electronics Research Laboratory
University of California, Berkeley, CA 94720

Longitudinal phenomena in a collisionless single-ended Q machine are simulated with the new bounded-plasma code PDW1 /1/. Simulations covering the four main parameter domains discussed in Ref. /2/ are presented. In the negative-bias domains, the monotonically decreasing and one-maximum potential distributions predicted by collisionless d.c. theory /2/ are recovered, with some quantitative disagreement arising from the filling of phase-space holes via numerical diffusion. The positive-bias domains usually exhibit the "potential relaxation instability", along with the moving double layers observed experimentally /3/. If, however, the cold-plate bias is raised above some critical value, the potential relaxation instability disappears, giving way to the one-minimum or monotonically increasing d.c. potential distributions predicted theoretically /2/. In these cases, the electron sheath in front of the cold plate occupies a significant portion of the interelectrode gap, which is in qualitative agreement with the experimental findings reported in Ref. /4/.

/1/ Wm.S. Lawson, User's Manual for the PDW1 Code, Plasma Theory and Simulation Group, E.R.L., U.C. Berkeley, CA 94720 (1983).

/2/ S. Kuhn, Plasma Phys. 23, 831 (1981).

/3/ S. Iizuka et al., Phys. Rev. Lett. 48, 145 (1982).

/4/ G. Popa et al., Phys. Lett. 87A, 175 (1982).

PARTICLE SIMULATIONS OF THE LOW-ALPHA PIERCE DIODE

T.L. Crystal and S. Kuhn[+])

Plasma Theory and Simulation Group
Electronics Research Laboratory
University of California, Berkeley, CA 94720

The evolution of small initial perturbations in the "classical" Pierce diode /1/ is simulated using the new bounded-plasma code PDW1 /2/. The simulations cover the parameter range $0 < \alpha < 3\pi$, where $\alpha = \omega_p L/v_o$. In the linear regime, potential profiles of the dominant eigenmode as well as oscillation frequencies of the next-to-dominant eigenmode are recovered and shown to be in excellent quantitative agreement with recent theoretical results /3/. In the linearly unstable cases, the nonlinear final state may be either a new, non-uniform d.c. state, or a state of large-amplitude oscillations. In particular, for $\alpha = 1.5\pi$ the final state is found to depend sensitively on the details of the initial conditions.

[+]) Permanent address: Institute for Theoretical Physics, University of Innsbruck, A-6020 Innsbruck, Austria.

/1/ J.R. Pierce, J. Appl. Phys. 15, 721 (1944).
/2/ Wm.S. Lawson, User's Manual for the PDW1 code, Plasma Theory and Simulation Group, E.R.L., U.C. Berkeley, CA 94720 (1983).
/3/ S. Kuhn, Memorandum UC3/ERL M83/61, E.R.L., U.C. Berkeley, CA 94720 (1983); to appear in Phys. Fluids.

**The Classical Pierce Diode: Using particle simulations on
linear & nonlinear behavior and final states**

T.L. Crystal, S. Kuhn*, and C.K. Birdsall.
EECS/ERL Cory Hall, Univ of Calif Berkeley CA 94720

The classical Pierce diode is a simple 1-d system of two
shorted metal plates, a cold beam of electrons injected
from one side and a neutralizing background of rigid ions.
While the plasma medium is technically stable, the finite-
ness of the Pierce system allows stable *and* unstable opera-
tion. It is usefully studied as an archetypical bounded-
plasma system, related e.g., to Q-machines, particle
accelerators, thermionic converters, and new high power
microwave sources; it can also serve to generate examples
of nonlinear, bifurcating (and oscillating) equilibria, virtual
cathodes and double-layers.

New particle simulations of the Pierce diode have success-
fully recovered many novel *linear* phenomena including the
dominant linear eigenmodes (seen in the internal electros-
tatic fields), and the dominant and *subdominant* eigenfre-
quencies, (seen both in the internal electrostatics *and* in
the external circuit current, $J_{ext}(t)$). These simulation
results conform very well to detailed predictions of a new
linear analysis[1].

The *final* (nonlinear) state recovered can show critical
dependence on *initial* (linear perturbation) conditions, and
can be made steady-state (d.c.) or periodic-oscillatory by
simply changing the initial conditions by a factor of $10^{**}-4$
or less. A third class of final state is also possible which has
oscillations which seem to be *nonperiodic*. Such oscilla-
tions occur in both the internal fields *and* the external
current, $J_{ext}(t)$; of course, they are device "useful" or "des-
tructive" depending on the electronics device being
modeled as a Pierce diode. The effects that external circuit
parameters have on the *linear* recovered (simulation)
behavior of the device are also found to be as predicted[1].

1 S. Kuhn. Submitted to *Phys. Fluids* 1984.

* On leave from the Univ of Innsbruck, Austria.

Axial Equilibria of Collisionless Single-ended Q-machines: particle simulations versus theory and experiment.

S. Kuhn*, P. Gray, T.L. Crystal, and C.K. Birdsall
EECS/ERL Cory Hall, Univ of Calif Berkeley CA 94720

Only recently has Q-machine equilibrium theory been systematically pushed to quantifiable predictions[1]. Now collisionless particle simulations have been run with the code **PDW1** in four main operating regimes (electron/ion rich emission, and positive/negative applied biases). For cases where the applied bias is negative, the simulations in fact recover *stable* final states as expected, having equilibrium potential profile *shapes* that agree with theory. But for cases with ion-rich emission, the simulated potential *values* can differ from analytic predictions because *equilibrium* ($\partial/\partial t = 0$) theory does not describe a system that has *evolved*; collisionless equilibrium theory finds phase space regions that are inaccessible to emitted particles, yet simulation shows that these regions are in fact *filled in Maxwell-Boltzmannly* during the system's evolution ($\partial/\partial t$ not 0) in reaching its eventual steady state. For positive applied bias, the simulations generally cannot recover the analytically expected equilibrium shapes, and instead indicate instability, whether the emission is electron rich or ion rich; these have character similar to the low frequency sheath oscillations (sometimes called[2] "false instabilities") and may also relate to the process of "charge domain formation" in Gunn oscillator theory[3].

Extended simulations also have suggested explanations for the experimentally observed (and overly mysterious) *high positive-bias stabilization*; raising the applied bias high enough turns the simulated potential profiles into simple Child-Langmuir diode profiles. Other recent experiments have reported seeing a so-called *moving double-layer* (which might better be re-named); we believe that these may be related to the "falsely unstable" sheath oscillations already alluded to here.

1 S. Kuhn, *Plasma Phys.*, **23**, 881 (1981).
2 N. Rynn, *Phys Fluids*, **9**, 165 (1966).
3 M.P. Shaw, H.L. Grubin, and P.R. Solomon, *The Gunn-Hilsum Effect*, Academic Press (1979), p.17.

* On leave from Univ of Innsbruck, Austria.

AN ANALYSIS OF SINGLE-WAVE PARTICLE ORBITS BASED ON CONSTANTS OF MOTION WITH APPLICATION TO SIMULATIONS OF THE ALFVEN ION-CYCLOTRON INSTABILITY

Niels F. Otani

Plasma Theory and Simulation Group, Electronics Research Laboratory,

University of California, Berkeley, CA 94720

Three exact constants of the motion have been found for particles moving in a single, circularly-polarized wave propagating along a uniform background magnetic field. The constant corresponding to the helical symmetry of the system fields, C, is of particular interest because it permanently restricts each particle to a relatively small region of $v_\perp$-v_z space which generally moves to higher v_z with increasing wave amplitude. Confinement of particles to one of these regions was verified in single-wave computer simulations of the Alfvén-ion-cyclotron instability. Existence of the three constants of motion reduces the problem to motion of the particle on a two-dimensional surface in $v_\perp$-v_z-ψ space. When the wave amplitude is slowly varying, the motion on this surface is characterized by the existence and slow time-scale motion of fixed points. At least one stable fixed point always exists and its deeply trapped particles exhibit an adiabatic invariant, namely, the action J. It is hypothesized that particle trapping, fixed point motion, and the existence of J may be responsible for the appearance of an edge in the v_z-distribution function shortly after wave saturation. The edge in the distribution function is also observed in some multiwave simulations, suggesting that some of the single-wave features of the particle motion may still be present even though the principal basis for the analysis, the conservation of C, is no longer valid.

Snapshot from a single-wave simulation of the Alfven ion-cyclotron instability showing the edge in the parallel velocity distribution and particle trapping in ψ, the gyrophase relative to the wave magnetic field.
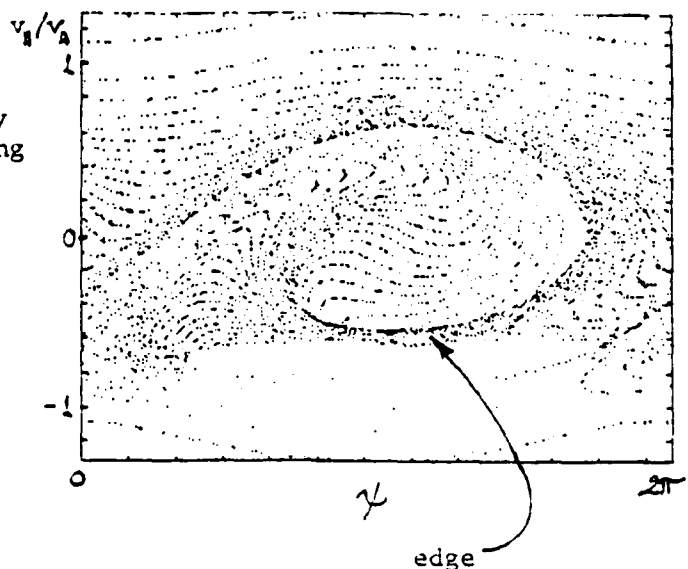
Beam-Driven Drift Instability in a Thermal Barrier Cell

V. A. Thomas

Electronics Research Laboratory, University of California,

Berkeley, CA 94720

W. M. Nevins

Lawrence Livermore National Laboratory,

Livermore, CA 91550

ABSTRACT

A low frequency instability ($\omega \ll \Omega_\alpha$) is sometimes seen in the **TMX-U** device at LLNL when the neutral beams are turned on in the thermal barrier cells. One possible explanantion is that a drift wave couples with beam modes from the injected ions in an unstable fashion. Our previous work for this instability (Bull. Am. Phys. **28** , Num. 8, 7Q5 (1983).) has been limited to the local approximation for both linear theory and particle simulations. We have now extended both the linear theory and the particle simulations to include a more complete treatment where the local approximation is *not* made. A comparison is given of the results obtained from the local approximation and the results obtained from using a nonlocal model. Even when the nonlocal and local growth rates are very close the instability may saturate in different fashions. Work supported in part by DOE and in part by ONR.

(5) V. A. Thomas and W. M. Nevins, "Simulation of the Ion-Beam Driven Drift Instability in a Magnetic Trap II," University of California, Berkeley, Memoranudm No. UCB/ERL M84/46, June 13, 1984.

(6) K-Y. Kim, "Vlasov-Poisson and Modified k-dV Theory and Simulation of Weak and Strong Double Layers," University of California, Berkeley, Memorandum No. UCB/ERL M84/47, June 1984.

Talks (abstracts on following pages)

(1) Sherwood Fusion Theory Conference, Lake Tahoe, April 11-13, 1984

    V. A. Thomas and W. M. Nevins, "Beam-Driven Drift Instability
       in a Thermal Barrier Cell."

    N. A. Otani, "An Analysis of Simple-Wave Particle Orbits Based
       on Constants of Motion with Application to Simulations of
       the Alfven-Ion-Cyclotron Instability."

(2) IEEE Conference on Plasma Science, St. Louis, May 14-16, 1984

    S. Kuhn, P. Gray, T. L. Crystal and C. K. Birdsall, "Axial Equilibria
       of Collisionless Single-Ended Q Machines: Particle Simulations
       versus Theory and Experiment."

    T. L. Crystal, S. Kuhn and C. K. Birdsall, "The Classical Pierce
       Diode: Using Particle Simulations on Linear and Nonlinear
       Behavior and Final State."

(3) International Conference on Plasma Physics, Lausanne, Switzerland,
    June 27-July 3, 1984

    T. L. Crystal and S. Kuhn, "Particle Simulations of the Low-Alpha
       Pierce Diode."

    S. Kuhn, C. K. Birdsall, T. L. Crystal, P. L. Gray, and W. S. Lawson
       "One-Dimensional Particle Simulations of the Collisionless Single-
       Ended Q Machine."

Reports

(1) V. A. Thomas and W. M. Nevins, "Electrostatic Ion-Ion Two-Streaming Insta-
    bility in a Thermal-Barrier Cell," University of California, Berkeley,
    Memorandum No. UCB/ERL M84/22, February 22, 1984.

(2) W. S. Lawson, "A Method for Simulation of Vlasov Systems with Discon-
    tinuous Distribution Functions and GASBAG User's Manual," University of
    California, Berkeley, Memorandum No. UCB/ERL M84/24, March 16, 1984.

(3) W. S. Lawson, "PDW1 User's Manual," University of California, Berkeley,
    Memorandum No. UCB/ERL M84/37, April 27, 1984.

(4) V. A. Thomas, W. M. Nevins, and Y-J. Chen, "Simulation of the Ion-Beam
    Driven Drift Instability in a Magnetic Trap I," University of California,
    Berkeley, Memorandum No. UCB/ERL M84/45, June 13, 1984.

Errata for *Plasma Physics via Computer Simulation* by Birdsall and Langdon:

Chap. 2, p. 10. In problem 2-2b, replace *Portis, 1979* by *Portis, 1978*.

Chap. 2, p. 14. In (8), both expressions $(t-\Delta t)/2$ should read $t-\Delta t/2$.

Chap. 2, p. 15. Below (12) the reference should be (*Boris, 1970b*).

Chap. 2, p. 17. In the third line, replace "Chapter 4, Section 4-14" with "Appendix D."

Chap. 2, p. 19. Problem 2-5c should read "..., and $NG/2-1$ independent values of Im $G(k)$ (sine coefficients)".

Chap. 3, p. 35. In (3) change E to E_{old}.

Chap. 3, p. 50. At the beginning of Section 3-14, delete "every time step."

Chap. 4, p. 59. Above (7), change citation to (*Boris, 1970b*).

Chap. 4, p. 65. At the beginning of Section 4-6, "Figure 2-6a, b, c" should be "Figure 2-6a, b." "Figure 2-6b, d" should be "Figures 2-6a(b), 2-6b(b)."

Chap. 4, p. 68. In 4-7(2), the factor Z' should be $Z'(\omega/(\sqrt{2}kv_t))$.

Chap. 4, p. 74. Replace E_k^2 everywhere by $|E_k|^2$. Below (2), read "As $\rho(x)$, $\phi(x)$ ..." Below (3), the phrase "If we" should begin a new sentence. In the seventh line from the bottom, replace "the $q\phi$ calculation" by "the $\rho\phi$ calculation."

Chap. 5, p. 87. The last line should continue "...and skip the ion motion, or make $m_i >> m_e$ (or $\omega_{pi} << \omega_{pe}$); then correctly ..."

Chap. 5, p. 92. below (5) remove the $\cos kx$ in the expressions for x_1 and v_{1}.

Chap. 5, p. 93. In Problem 5-5b, the first reference should be *Taylor and McNamara* (1971).

Chap. 5, p. 94. Change citation to *Huieff* (1949).

Chap. 5, p. 109. Figure 5-9c(d), $\phi(x)$ axis numbering should be 0.3, 0.2, 0.1, 0, -0.1, -0.2.

Chap. 5, p. 115. Below (5), change citation to (*Lee and Birdsall, 1979a, b*)

Chap. 6, p. 136. In the first paragraph, change citation to *Godfrey and Langdon* (1976).

Chap. 6, p. 138. In the first paragraph, change citation to *Boris* (1970b).

Chap. 7, p. 150. In (2), change x/x to x.

Part Two, p. 154. In the last paragraph, replace "is essentially" with "is drawn in part from "

Chap. 8, p. 162. In (7), the summand should be $P(k)$.

Section 8-5, p. 162. 3 lines above (2), replace the "or" in "... form or smoothing ..." with "of."

Chap. 8, p. 173. Below (13), change 8-7(8) to 8-7(4).

Chap. 8, p. 181. In Problem 8-13b, remove the squares from the ω's. In Problem 8-13c, change "this instability" to "the instability of this Section."

Chap. 9, p. 200. In the second paragraph, change the citation to *Buneman, 1967.*

Section 10-1, p. 213. Add: "This chapter draws heavily on *Langdon* (1973)."

Chap. 12, p. 265. In Problem 12-3d, $j' = j$ should be $j' \neq j$.

Chap. 13, p. 301. The citation *Tetreault, 1983* should be *Berman et al., 1983*

Chap. 14, p. 348. Equation (5) was derived using (6) which does not always hold. The potential due to external charge must be handled separately; see Section 10-4 and *Decyk* (1982).

Chap. 15, p. 358. In the last line, replace "second next section" with "Section 15-8".

Chap. 15, p. 360. In the paragraph beginning "Methods for ...", replace "discussed in the next Section" with "discussed in Section 15-8."

Chap. 15, p. 366. In (3b), $\sin ck\Delta t/2$ in the E^n term should be $\sin ck\Delta t$. In paragraph preceding problem, replace $\alpha(kv)$ with $\alpha(k)$

Chap. 15, p. 371. Above (10), change the citation to *Lindman* (1975).

Section 15-16, p. 381. The citation in the 3rd paragraph should be *Brackbill and Forslund* (1985)

Chap. 15, p. 383. Above (a), the citation *Katamura* (1980) should be *Katamura* (1981).

Chap. 16, p. 407. All four of the α terms should be $|\alpha \cdot k|$ instead of $|\alpha|$.

Chap. 16, p. 413. The parenthetical comment at the end of the second paragraph should appear after "vanishes" in the previous sentence.

Appendix A, p. 422. In two places, change citation to *Cooley, Lewis and Welch* (1970).

References. In the first printing, add the following references:

Denavit, J., "Pitfalls in Particle Simulations and in Numerical Solutions of the Vlasov Equation," *Methoden und Verfahren de Mathematischen Physik,* **20**, Peter Lang, 247-269, 1980.

Sköllermo, A., "A Better Difference Scheme for the Laplace Equation in Cylindrical Coordinates," *J. Comput. Phys.* **47**, 160-163, 1982.

Sköllermo, A., and G. Sköllermo, "A Fourier Analysis of Some Difference Schemes for the Laplace Equation in a System of Rotation Symmetry," *J. Comput. Phys.* **28**, 103-114, 1978

PLASMA
PHYSICS
VIA COMPUTER
SIMULATION

Charles K. Birdsall

Electrical Engineering and Computer Sciences Department
University of California, Berkeley

A. Bruce Langdon

Physics Department, Lawrence Livermore Laboratory
University of California, Livermore

CONTENTS

SECTION III: BOOK, JOURNAL ARTICLES, REPORTS, VISITORS, TALKS

Book   <u>Plasma Physics via Computer Simulation</u>
       by Charles K. Birdsall and A. Bruce Langdon
       was completed in this period. Considerable thanks are due
       to DOE for encouragement and support, starting with the original
       notes (begun about 1972), through to final book preparation.
       Following are: book Contents, Errata and ordering information.
       (Be persistent with McGraw-Hill; the book is <u>not</u> out of print!
       Let Professor Birdsall know of any such replies.)

A. PDW1: Particle Simulation of Non-periodic Systems

Wm. S. Lawson

The development and documentation of the PDW1 code (for Plasma Device Workshop) has now been completed. The code is debugged, and fully documented. It is available to users of the National Magnetic Fusion Energy Computer System on line, and the user's manual is avaliable from the Plasma Theory and Simulation group as memo UCB/ERL M84/37. Documentation includes descriptions of important variables, subroutines and flow charts, as well as examples of input files and the resulting output.

PDW1 is a general purpose particle simulation code which is capable of handling non-periodic boundary conditions and a simple RLC external circuit. A large variety of input parameters exist, allowing one to specify the usual parameters of periodic simulations, plus: thermal, drift, and cut-off velocities for the injected distributions; DC and AC external biases in the circuit; and injected currents. The code works in one spatial dimension, and either one, two, or three velocity dimensions. A magnetic field is allowed in the two and three velocity dimension cases, and it is allowed to be at any angle in the x-z plane in the three velocity dimension case.

PDW1 and modifications of PDW1 are already in much use at our Plasma Theory and Simulation group. It has been used, and is being used, to simulate many interesting problems, such as the Pierce Diode, double layers, Q-machines, plasma-wall interactions, and oblique electron Bernstein waves.
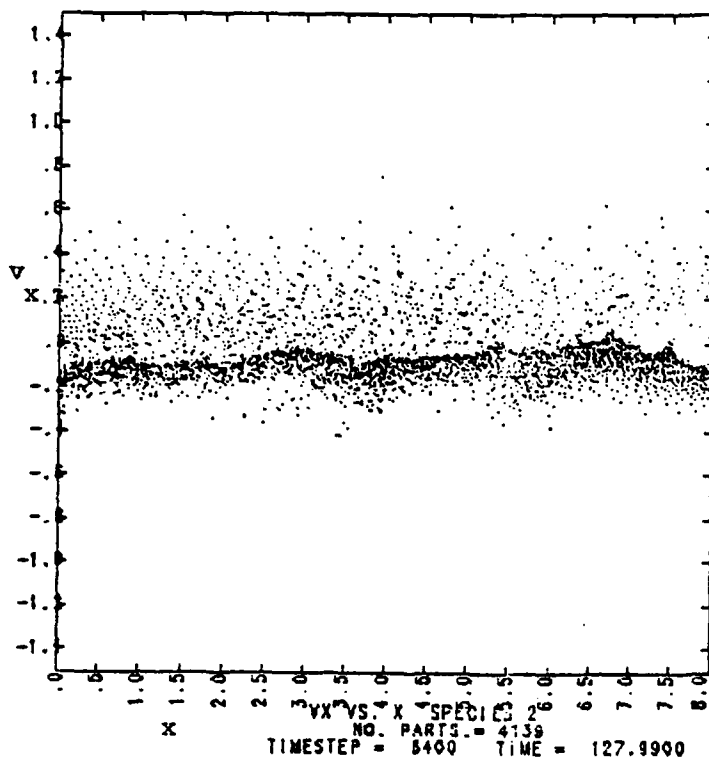
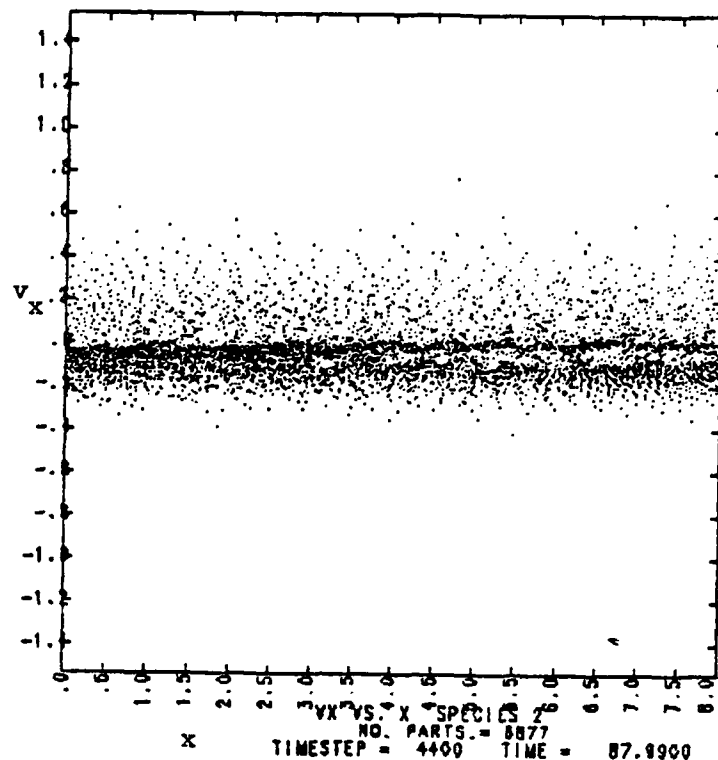Figure 1. v_x vs. x for empty start case. $t = 128$.

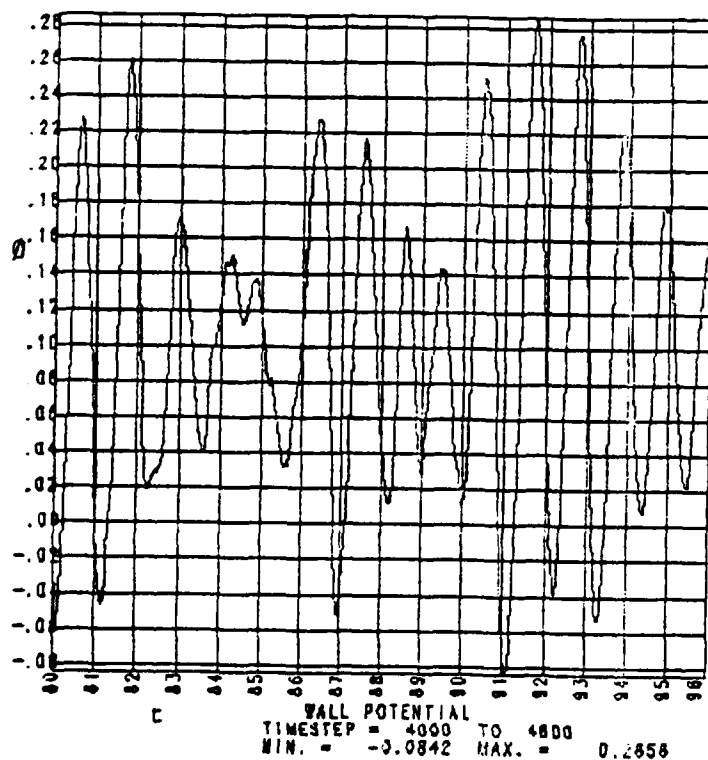Figure 2 v_x vs. x for full start case. $t = 88$.

Figure 3 Full start case. Time evolution the right wall potential, from $t = 80$ to $t = 96$.
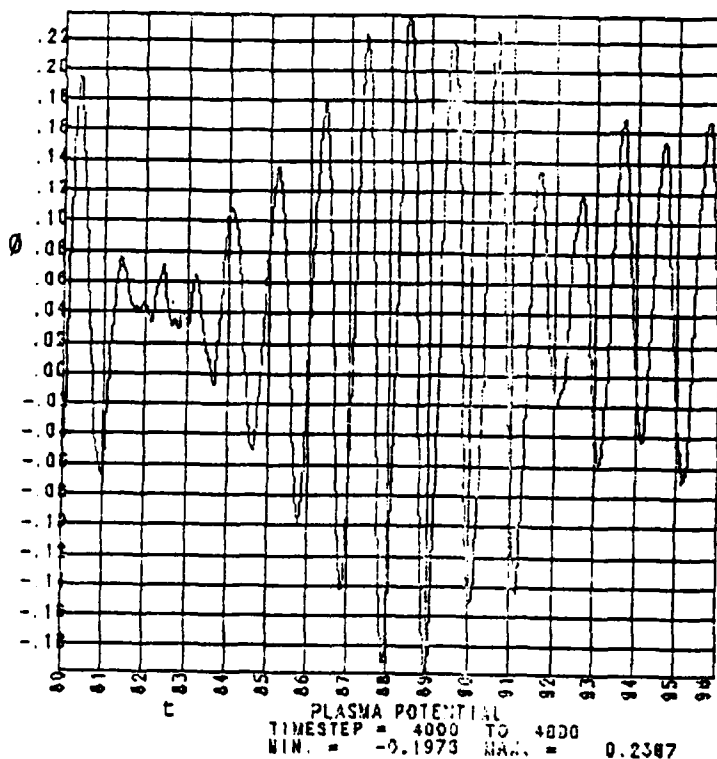

Figure 4 Full start case. Time evolution of the plasma potential, from $t = 80$ to $t = 96$.

All are for $T_i/T_e = 1$, $T_{eh}/T_{ec} = 4$ $L = 8$, $m_i/m_e = 25$

DISTRIBUTION LIST

Department of Energy
Hitchcock. Katz. Lankford. Nelson.
Sadowski

Department of Navy
Condell. Florance. Roberson

Austin Research Associates
Drummond. Moore

Bell Telephone Laboratories
Hasegawa

Cal. Inst. of Technology
Liewer. Bridges. Gould

Calif. State Polytech. Univ.
Rathmann

Cambridge Research Labs
Rubin

Columbia University
Chu

E. P. R. I.
Scott

General Atomic Company
Bernard. Helton. Lee

Hascomb Air Force Base
Rubin

Hughes Aircraft Co., Torrance
Adler. Longo

Hughes Research Lab, Malibu
Harvey. Poeschel

JAYCOR
Hobbs. Klein. Tumolillo. Wagner

Kirtland Air Force Base
Pettus

Los Alamos National Lab.
Barnes. Borovsky. Forslund. Kwan.
Lindemuth. Mason. Mostrom. Nielson.
Oliphant. Sgro. Thode

Lawrence Berkeley Laboratory
Cooper. Kaufman.Kim. Kunkel. Lee.
Pyle

Lawrence Livermore National Lab
Albritton. Anderson. William Barr.
Brengle. Briggs. Bruijnes. Byers.
Chambers. Chen. B. Cohen. R. Cohen.
Denavit. Estabrook. Fawley. Friedman.
Fries. Fuss. Harte. Hewett. Killeen.
Kruer. Langdon. Lasinski. Maron.
Matsuda. Max. Nevins. Nielsen.
Smith. Tull

Mass. Inst. of Technology
Berman. Bers. Gerver.

Mission Research Corporation
Godfrey

Naval Research Laboratory
Boris. Craig. Haber. Orens. Winsor

New York University
Grad. Harned. Weitzner

Northeastern University
Silevitch

Oak Ridge National Lab.
Dory. Meier. Mook

Princeton Plasma Physics Lab
Chen. Cheng. Lee. Okuda. Tang.
Graydon

Sandia Labs, Albuquerque
Freeman. Humhries. Poukey.
Quintenz. Wright

Sandia Labs, Livermore
Marx

Science Applications, Inc.
Drobot. Mankofsky. McBride. Siambis.
Smith

Stanford University
Blake. Buneman

University of Arizona
Morse

University of California, Berkeley,
Arons. Chorin. Grisham. Hudson.
Keith. Lichtenberg. Lieberman.
McKee. Morse. Birdsall. Lawson.
Otani. Theilhaber. Wendt

University of California, Davis
DeGroot. Woo

University of California, Irvine
Rynn

University of California, Los Angeles
Dawson. Decyk. Huff. Lin

University of Iowa
Knorr. Nicholson

University of Maryland
Gillory. Rowland. Winske

University of Pittsburgh
Zabusky

University of Texas
Lebouef. Horton. McMahon. Tajima

Institute of Fusion Studies
Librarian

University of Washington
Potter

University of Wisconsin
Shohet

Varian Associates
Helmer

Bhabha Research Centre
Aiyer. Gioel

Culham Laboratory
Eastwood

Ecole Polytechnique, Lausanne
Hollenstein. Rousset

Ecole Polytechnique, Palaiseau
Adam

Centro de Electrodinamica, Lisbon
Brinca. Crystal

Kyoto University
Abe. Jimbo. Matsumoto

Nagoya University
Kamimura

Max Planck Inst. für Plasmaphysik
biskamp. Kraft. Chodura

Osaka University
Mima. Nishihara

Oxford University
Allen

Riso National Labs
Lynov. Pecseli

Tel Aviv University
Cuperman

Tohoku University
N. Sato

Universität Bochum
Schamel

Universität Innsbruck
Cap. Kuhn

Universität Kaiserslautern
Wick

University of Reading
Hockney

University of Tromso
Trulsen. Armstrong

END

FILMED

8-85

DTIC